An All-in-One Rapid Prediction of Ground Motion Intensity Measures Hybrid Network for Multi-Task in The North-South Seismic Belt of China

Qingxu Zhao[1], Mianshui Rong[1], Bin Zhang[2], Xiaojun Li[1]

[1]Key Laboratory of Urban Security and Disaster Engineering of China Ministry of Education, Beijing University of Technology, Beijing, China, 100124

[2]Institute of Earthquake Forecasting, China Earthquake Administration, Beijing, China, 100036

Corresponding author: Mianshui Rong (rongmianshui@bjut.edu.cn)

Key Points:

- CRAQuaek: a model for the simultaneous prediction of six different intensity measures based on data-driven techniques
- Model performance tested by earthquake events in the north-south seismic belt of China
- The model can improve accuracy and timeliness as the input seismic wave is continuously updated

Abstract

The north-south seismic belt of China poses a high risk of earthquakes, necessitating the need for accurate and rapid prediction of intensity measures (IMs) to prevent and mitigate potential damage. We have developed a new multi-task model, CRAQuake, to predict IMs for the north-south seismic belt of China. Using initial arrival seismic waves recorded at a single station as input, CRAQuake simultaneously predicts six IMs without relying on pre-configured parameters such as earthquake source, path, and location. The model was trained on 4281 sets of strong motion records datasets at 822 stations and tested to show highly correlated results with the target IMs. The prediction performance continues to improve as the input initial arrival seismic wave time window increases. CRAQuake promises to enhance the accuracy and timeliness of IMs prediction in the north-south seismic belt of China.

Plain Language Summary

The north-south seismic belt of China, a region at high risk for earthquakes, necessitates the accurate and rapid prediction of earthquake intensity measures (IMs) to minimize potential damage. We have developed a powerful tool, CRAQuake, to address this critical need. This advanced model leverages initial seismic waves recorded at a single station to simultaneously predict six different IMs without relying on preset information like earthquake source, path, or location. Trained on a vast dataset of strong motion records from 822 stations, our testing has shown that CRAQuake's predictions are highly aligned with the actual IMs. Furthermore, increasing the time window of the initial seismic waves used as input significantly improves the model's prediction accuracy. With CRAQuake, we can look forward to more accurate and timely predictions of IMs in the north-south seismic belt of China, empowering us to better prepare for and respond to earthquakes.

1 Introduction

Assessing the damage caused by earthquakes is a crucial task for earthquake early warning systems (EEWs). This assessment is necessary for emergency disaster response and providing early warning information to the public (R. M. Allen & Melgar, 2019; Cremen & Galasso, 2020; Zollo et al., 2023). However, it can be challenging to determine the severity of an earthquake based solely on the seismic waves it generates. To address this challenge and reduce the damage caused by earthquakes, researchers have proposed using intensity measures (IMs) to quantify the impacts of ground motion. Currently, there are several IMs in use, such as Peak Ground Acceleration (PGA), Peak Ground Velocity (PGV), Peak Ground Displacement (PGD), and Spectral Acceleration (SA). These IMs characterize the amplitude and spectral properties of ground motion. IMs have contributed significantly to the development of EEWs, so rapid and precise prediction of IMs is essential for EEWs.

There are currently two primary methods for predicting IMs during an earthquake. The first method involves using a Ground Motion Prediction Equation (GMPE) or Ground Motion Models (GMMs). This method is commonly used in regional EEWs (Zollo et al., 2009; Cremen & Galasso, 2020). Researchers have successfully established GMPE or GMMs for predicting IMs by using seismic data from various regions (K. Campbell & Bozorgnia, 2008; Bindi et al., 2011; K. W. Campbell & Bozorgnia, 2014; Du & Ning, 2021). This method is advantageous as it uses information from more ground motion stations near the epicenter and, as a result, provides

more accurate predictions. However, regional EEWs may need help with delays in receiving and analyzing initial seismic waves from various stations. This delay can create "blind zones" for early warning as there may not be sufficient time to issue warnings before the arrival of destructive seismic waves (R. Allen et al., 2009; Caruso et al., 2017). Additionally, determining earthquake source parameters during seismic events proves challenging. For instance, the magnitude cannot be accurately measured due to the saturation of large earthquakes (Kanamori, 2005; Wu & Zhao, 2006; Peng et al., 2017; Y. Wang et al., 2021), and the fault distance cannot be obtained before the fault ruptures, hindering the accuracy and timeliness of GMPE predictions. Another approach involves using empirical formulas that rely on seismic wave features and IMs. This method is commonly utilized in on-site EEWs and has been studied extensively (Wu & Kanamori, 2005; Wu et al., 2007; Wu & Kanamori, 2008; Zollo et al., 2010; Peng et al., 2013; Liu C. et al., 2019). By analyzing the initial arrival of seismic waves from a single station, this approach can predict IMs and issue early warning messages even in areas close to the earthquake epicenter. Compared to GMPE, this method is timelier and allows longer emergency response times in the target region (Peng et al., 2017). However, it may result in slightly lower prediction accuracy due to the limited amount of information that can be utilized. Additionally, because empirical formulas require human extraction of characteristic parameters, there is a risk of subjectivity and one-sidedness, which can lead to errors and limit the accuracy of the predictions.

In recent years, Advances in science and technology have led to the gradual application of data-driven methods to earthquake engineering, which have yielded impressive outcomes (Mousavi & Beroza, 2022a, 2022b; Hajian et al., 2023). By analyzing vast data, data-driven approaches can uncover hidden patterns and laws, leading to accurate and widely applicable predictions. In the field of earthquake engineering, popular data-driven methods include machine learning techniques like Support Vector Machines (SVM), as well as deep learning methods such as Convolutional Neural Networks (CNN), Recurrent Neural Networks (RNN), and Self-Attention Mechanism (SAM). Table 1 summarizes the practical uses of different data-driven techniques in earthquake engineering. Table S1 of the supplementary Information also shows the input information and data sources used for the data-driven model in Table 1. It is worth noting that many researchers are also employing data-driven methods to predict IMs, which can be categorized into two types: first type methods that use earthquake sources, paths, and site parameters as inputs(Fayaz et al., 2021; Hu et al., 2022; Fayaz & Galasso, 2022a; Fayaz et al., 2023), similar to GMPE methods, inability to meet timeliness requirements, and another type methods that use seismic wave or P-wave features as inputs(Dai et al., 2024; Hsu et al., 2013; Jozinović et al., 2020; Y. Liu et al., 2024; Y. Wang et al., 2023). Using P-wave features as inputs can lead to human empirical and subjectivity, affecting the accuracy of prediction results. These studies are incredibly significant in advancing the prediction of IMs, but there is still room for improvement in these methods. For instance, most methods are single-task and can only predict one type of IMs, except the Jozinović et al. study (Jozinović et al., 2020). However, predicting a single IMs is insufficient for earthquake engineering and mitigation efforts because of the complexity of ground motion. Additionally, although there are numerous data-driven models for predicting IMs, none exist for multitasking prediction of IMs in the north-south seismic belt of China. As accurate post-earthquake prediction of IMs is crucial for minimizing seismic hazards in this region, it is imperative to develop a rapid and precise method for predicting IMs in the north-south seismic belt of China.

This study introduces a novel approach (CRAQuake) to predicting IMs in the north-south seismic belt of China. The CRAQuake model combines advanced data-driven techniques (CNN, RNN, and SAM) to predict six types of IMs (PGA, PGV, PGD, and SA at 0.3, 1, and 3 s periods) directly from initial seismic waves without requiring pre-configure of earthquake sources, paths, or site parameters. CRAQuake was trained, validated, and tested on strong motion data from China's north-south seismic belt. Test results show that CRAQuake can rapidly, accurately, and objectively predict IMs, eliminating human subjectivity and empiricism. The IMs predicted by CRAQuake are extremely important for earthquake early warning and have a non-negligible reference value for emergency disposal of some critical projects.

Table 1. A brief review of some examples in the field of earthquake engineering using data-driven methods

Approach	Applications in Earthquake Engineering	Reference
SVM	Prediction IMs (PGA)	(Hsu et al., 2013)
	Prediction IMs (Arias intensity, IA; cumulative absolute velocity, CAV; and significant duration, Ds)	(Hu et al., 2022)
XGBoost	Prediction IMs (SA)	(Dai et al., 2024)
CNN	Magnitude estimation	(Y. Wang et al., 2022)
	Prediction IMs (CAV)	(Y. Wang et al., 2023)
	Site classification	(Ji et al., 2023)
	Prediction IMs (PGA, PGV, SA)	(Jozinović et al., 2020)
	Prediction IMs (PGA)	(Y. Liu et al., 2024)
RNN	Predict earthquake site response.	(Zhu et al., 2023)
	Prediction IMs (PGA)	(A. Wang et al., 2023)
	Prediction IMs (Ds, CAV, IA, SA)	(Fayaz et al., 2021)
	Prediction IMs (Ds, CAV, IA, PGA, PGV, SA)	(Fayaz & Galasso, 2022b)
	Prediction IMs (Ds, IA, PGA, PGV, SA)	(Fayaz et al., 2023)
SAM	Magnitude estimation and Earthquake location	(Münchmeyer et al., 2021)
	Earthquake detection and phase picking	(Mousavi et al., 2020)

2 Methods and data

2.1 Basic information about CRAQuake

As previously mentioned, the CRAQuake model was developed using a combination of CNN, RNN, and SAM techniques, each with unique advantages. CNN extracts response features from input species, with increasing network depth allowing for more specific and advanced feature learning. RNN is better suited for time series data and has a memory function, enabling the model to consider previous information when processing current input. SAM captures dependencies between different locations in the time domain sequence, improving correlation understanding between other places in the input sequence and prediction accuracy. The CRAQuake model leverages these strengths to enhance the timeliness and accuracy of IM predictions. For brevity, we will focus on our model without delving into the basics of CNN, RNN, and SAM, which can be found in published literature (Hochreiter & Schmidhuber, 1997; Lecun et al., 1998; Chung et al., 2014; Vaswani et al., 2017).

The multitask IMs prediction network called CRAQuake is illustrated in Figure 1. The input to the network is a tridirectionally acceleration record ($H \times W \times 1$), where H is the number of channels, which is 3, and W is the length of the input seismic wave. For instance, if the input is an initial arrival seismic wave of 1 second (with a sampling frequency of 100 Hz), W is 100. The input acceleration is initially processed through a sequence folding layer to enable independent convolution operation. The convolution module then performs feature extraction on the input acceleration. The convolution module consists of a convolution layer, a ReLU activation layer, and a maximum pooling layer, as shown in the first figure at the bottom of Figure 1. The sequence unfolding layer restores the features extracted by the convolution module to a sequence structure so that the recurrent neural network module can process the extracted features. The RNN block, shown in the second diagram at the bottom of Figure 1, contains an LSTM and GRU layers. The processed features are then entered into the self-attention module, the SAM block, as shown in the third diagram at the bottom of Figure 1. The SAM block consists of a self-attention layer, a layer norm layer, and a dropout layer. The module adaptively assigns weights to the features and prevents overfitting. Finally, the FC block performs regression calculations on the features to output the results. The FC block has three fully connected layers and outputs 6 IMs: PGA, PGV, PGD, and SA, at 0.3, 1, and 3 s periods. The base-10 logarithm has been applied to all the IMs (i.e., $\log_{10}$IMs). The detailed architecture and hyperparameter settings of CRAQuake are listed in Table S2 of the Supplementary Information.

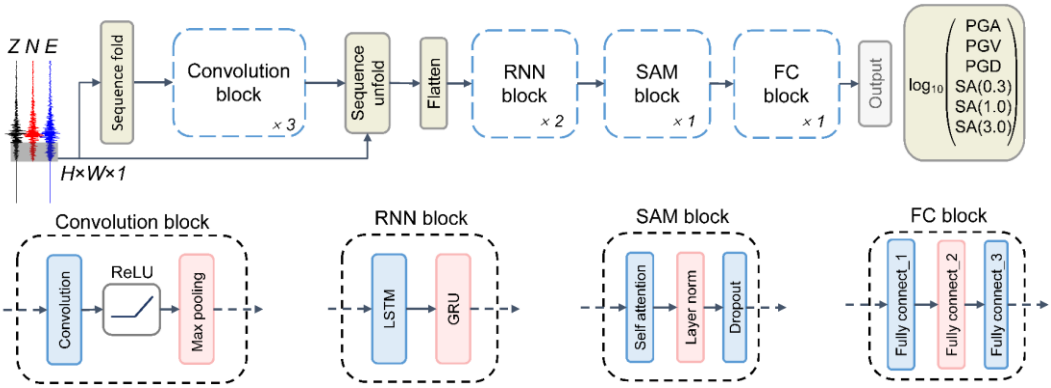

Figure 1. Architecture of the CRAQuake.

It is worth noting that selecting the architecture and hyperparameters is a tedious process. The architecture and hyperparameters were tried and determined during the selection process through iterations. As an example of choosing the dropout rate, the CRAQuake architecture and hyperparameters were set regularly, and the validation loss was tested using 13 different dropout rates (Supplementary Information Figure S1). The results showed that the validation loss was lowest when the dropout rate was 0.2. Therefore, the dropout rate of CRAQuake was set to 0.2, and the remaining architectures and hyperparameters were also developed similarly. Thus, the architecture and hyperparameters of CRAQuake are only the best ones tested.

2.2 Ground-motion data (Input features)

To create a reliable model for predicting ground motion intensity in the north-south seismic belt of China, we collected data from 781 seismic events in the area (Figure 2a). The data was recorded by 822 stations (Figure 2b), resulting in 4281 sets of acceleration records, all with magnitudes (surface wave magnitude, Ms) equal to or greater than 3. You can find more

detailed information in the Supplementary Information, Table S3. We processed the data by performing routine tasks such as baseline correction, unification of the sampling frequency to 100 Hz, and automatic selection of P-wave arrivals followed by manual calibration. The dataset was then divided according to the earthquake occurrence time into training, validation, and testing datasets to ensure that the records from the same earthquake were included in the same dataset. The details of the dataset division are available in the Supplementary Information, Table S4. The training dataset is used to train CRAQuake. The validating dataset is used to optimize the architecture and hyperparameters of CRAQuake. The testing dataset is used to test CRAQuake in predicting IMs. Supplementary Information Figure S2 illustrates the magnitude distribution of the acceleration records in different datasets.

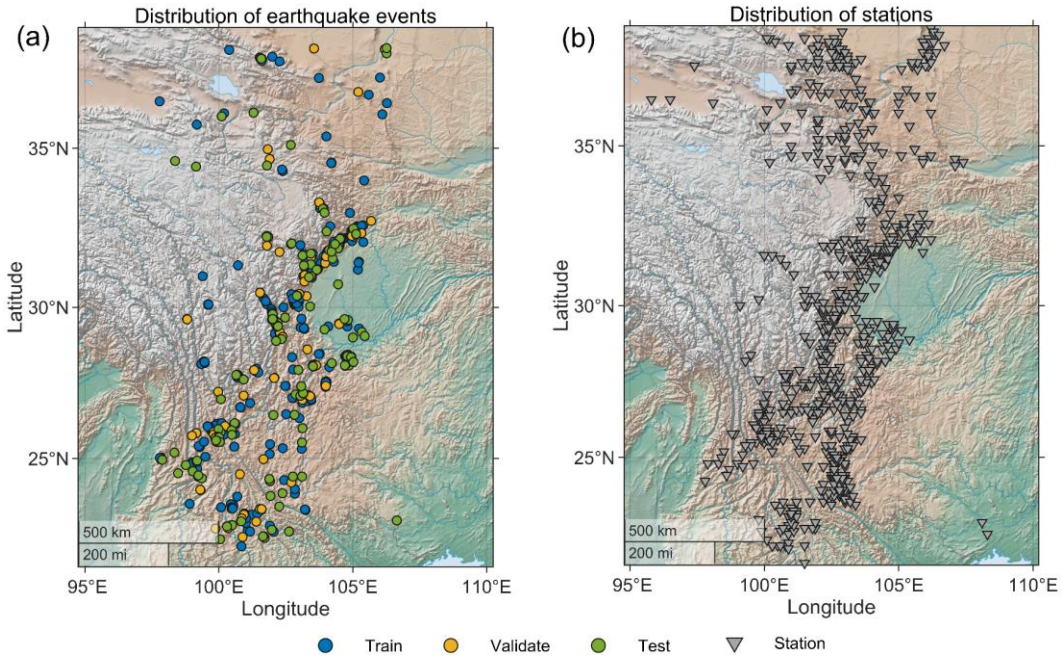

Figure 2. Distribution of earthquake events used (a) and stations (b).

2.3 Intensity measurements (Target)

CRAQuake produces a set of IMs for each group acceleration record, including PGA, PGV, PGD, and SA at 0.3, 1, and 3s periods. PGA and PGV are the targets due to their high correlation with earthquake intensity and damage. For instance, current EEWs rely mainly on PGA and PGV predictions to identify earthquake damage (Wald et al., 1999; Cremen & Galasso, 2020). After PGA or PGV predictions have been made, intensity or comparison thresholds can be calculated from these parameters to predict the potential damage caused by earthquakes accurately (Festa et al., 2017; Hsu et al., 2018; Satriano et al., 2011). Furthermore, in China, the China Earthquake Administration calculates instrumental intensity using PGA and PGV(China Earthquake Administration, 2020). PGD was chosen as the target due to its ability to represent low-frequency ground motion, significantly impacting long-period structures. Accurately predicting PGD is crucial for analyzing seismic hazards in medium and long-period structures with varying site conditions and designing earthquake-resistant engineering structures (Zhang et al., 2021). Similarly, SA was selected as it can effectively characterize ground-motion features as a single-degree-of-freedom (SDoF) system, considering factors such as acceleration, structural

self-resonance frequency, and damping ratio (Bazzurro et al., 1998). Real-time prediction of SA is of utmost importance for earthquake engineering applications, and we have chosen to predict SA values for three periods: 0.3 s, 1 s, and 3 s. Figure 3 and Figure 4 illustrate the distribution of IMs in terms of magnitude and epicenter distance.

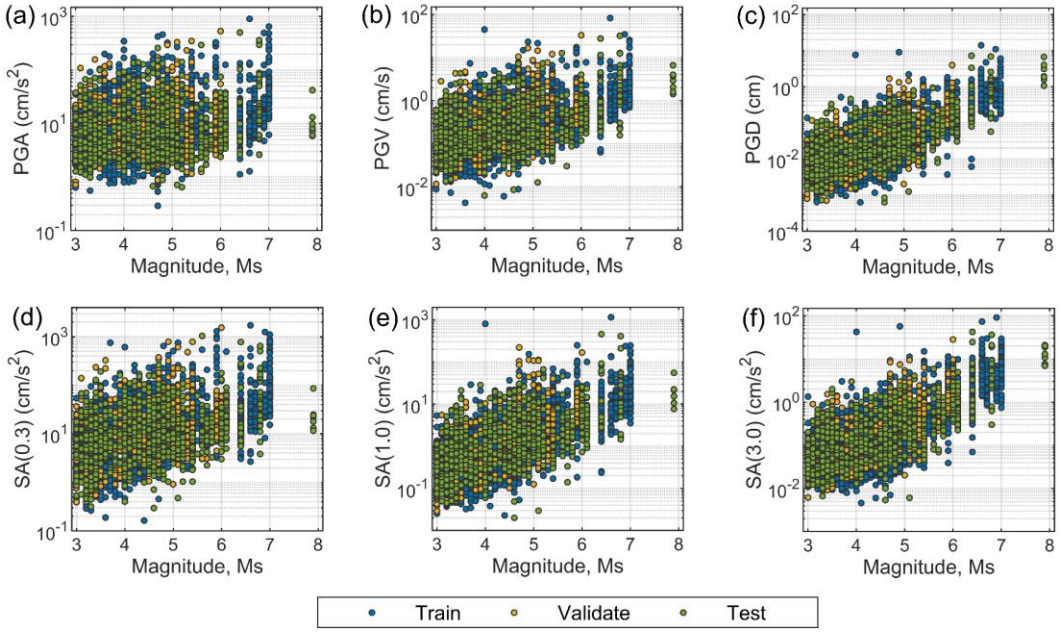

Figure 3. Distribution of ground motion parameters with magnitude.

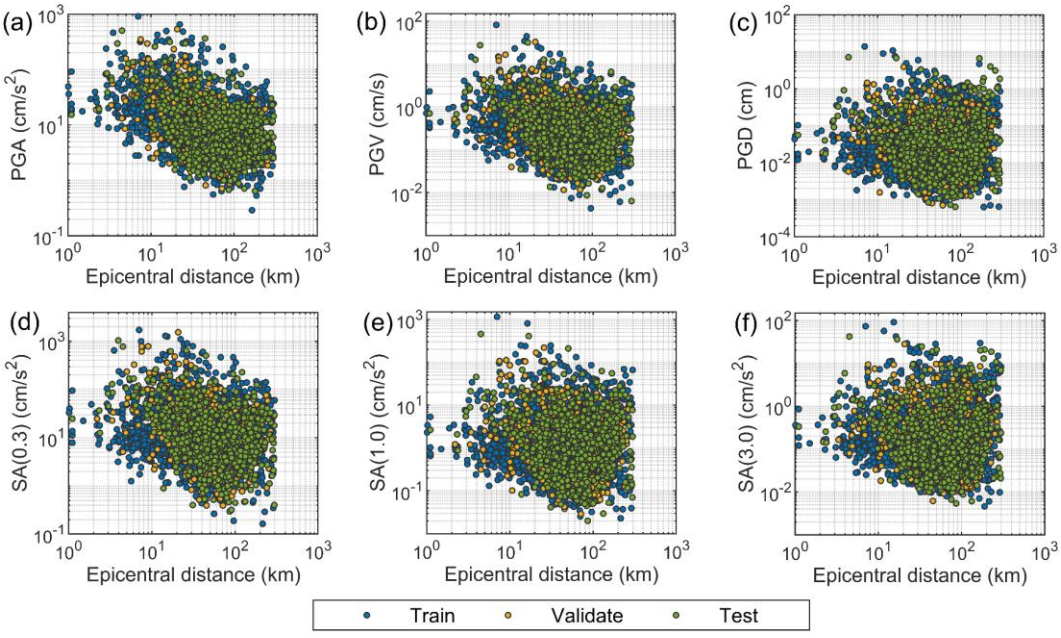

Figure 4. Distribution of ground motion parameters with epicentral distance.

2.4 Model development

The CRAQuake model was trained using data from the north-south seismic belt of China. The model utilized the root mean square error (RMSE) as the loss function, comparing target and predicted values. The training was performed using the adaptive moment estimation (Adam) optimizer (Kingma & Ba, 2017) with a learning rate of 10^{-3} and a batch size of 80. The training process was stopped after 200 epochs or if the validation loss did not decrease for 20 consecutive rounds. As the number of training rounds increased, the training and validation loss curves converged, and the final model was selected based on the lowest validation error. Please refer to Figure S3 for more details.

3 Model performance

3.1 Evaluation indicators

To assess the performance of CRAQuake, we utilized the Pearson correlation coefficient (PCCs) and standard deviation of residuals (STD) to evaluate CRAQuake prediction results, as illustrated in the following equation. In Equation (1), PCCs refer to the Pearson correlation coefficient, where Y_{Tra} represents the target value, Y_{Pre} represents the predicted value, and n is the number of samples. The value of PCCs ranges from -1 to 1, with a closer value to 1 indicating a better degree of linearity. A PCCs in the range of 0.3 to 0.5 shows a low correlation, while a PCCs in the range of 0.5 to 0.7 suggests a medium correlation. PCCs in the range of 0.7 to 0.9 indicate a high correlation. Equation (2) defines Res as the residuals of the predicted IMs for each acceleration record group. In contrast, Equation (3) defines STD as the standard deviation of the residuals, where u is the mean of the predicted IMs residuals and n is the number of samples. STD reflects the degree of dispersion of the predicted residuals, with a minor STD indicating higher prediction accuracy.

$$\mathrm{PCCs} = \frac{\sum_{i=1}^{n}\left(Y_{Tra,i} - \overline{Y_{Tra}}\right)\left(Y_{Pre,i} - \overline{Y_{Pre}}\right)}{\sqrt{\sum_{i=1}^{n}\left(Y_{Tra,i} - \overline{Y_{Tra}}\right)^2}\sqrt{\sum_{i=1}^{n}\left(Y_{Pre,i} - \overline{Y_{Pre}}\right)^2}} \tag{1}$$

$$\mathrm{Res}_i = log_{10}\left(Y_{Pre,i}\right) - log_{10}\left(Y_{Tra,i}\right) \tag{2}$$

$$\mathrm{STD} = \sqrt{\frac{\sum_{i=1}^{n}\left(\mathrm{Res}_i - u_i\right)^2}{n}} \tag{3}$$

3.2 Input time window length

When deciding on the appropriate input time window (TW) length, it is essential to balance timely warnings with accuracy in practical applications. Typically, warning information is calculated and released once the station monitors a P wave of 3 seconds (Kanamori, 2005; Wu & Zhao, 2006; Hsiao et al., 2009; Peng et al., 2017; Y. Wang et al., 2021). However, increasing

the TW length can provide more ground motion information. To analyze the effectiveness of CRAQuake in predicting IMs, we started with a TW length of 3 seconds and carefully examined the results. We then gradually increased the TW length and tested the model's ability to predict IMs continuously.

3.3 Predictive performance of the model at 3s Tw on the test dataset

The performance of CRAQuake in predicting IMs at 3 s TW in the test dataset was evaluated. Figure 5 displays the linear distribution of the predicted values of IMs versus the target values of IMs. Each solid circle in the figure represents an expected value, while the black solid line is the 1:1 line, and the two black dashed lines are the ± STD. Different colors represent other magnitudes, with darker colors indicating smaller magnitudes and lighter colors representing larger magnitudes. The predicted values of IMs are uniformly distributed on both sides of the 1:1 line without any significant underestimation or overestimation. However, the predicted values of PGD are slightly underestimated when the magnitude is considerable (Figure 5c). All six IMs have high PCCs, with values greater than 0.7, indicating a strong correlation. PGD has the highest PCCs of 0.83, while the lowest PCCs of 0.78 is for SA (0.3).

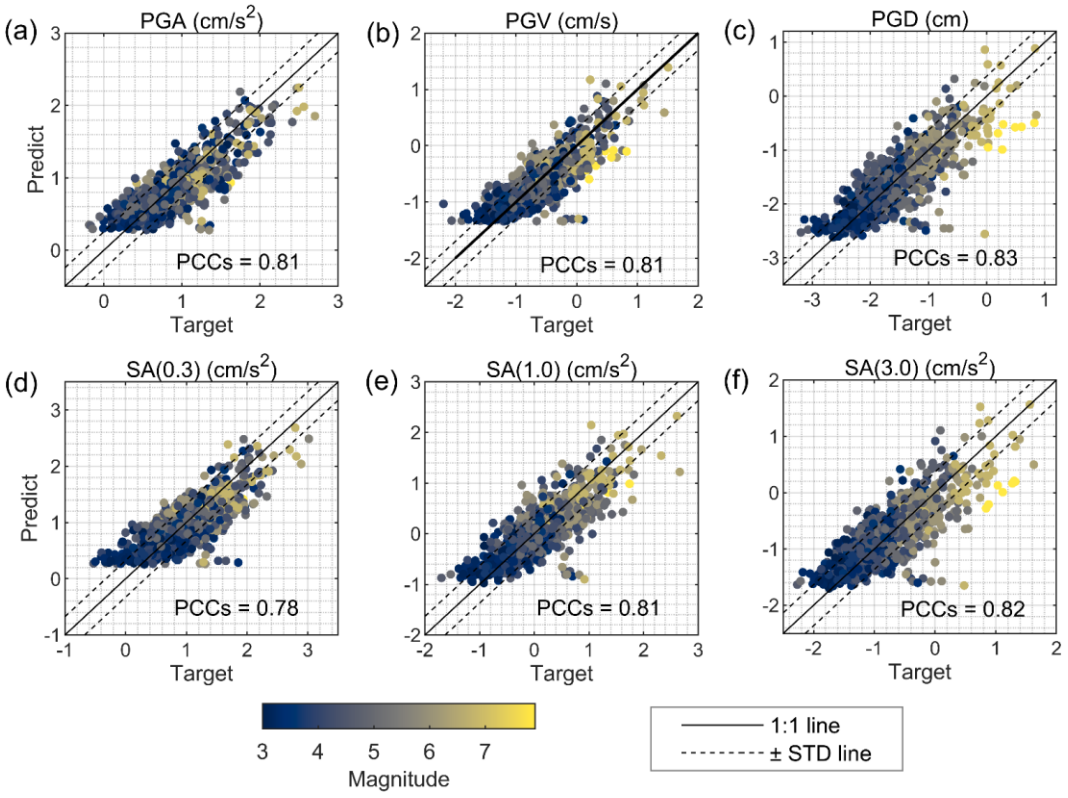

Figure 5. The linear relationship between IMs Target values and predicted values when TW is 3s.

Figure 6 displays the distribution of residuals of IMs based on epicenter distance predicted by CRAQuake on the test dataset when the TW is 3s. Each gray dot in the figure represents a residual, and the two black solid lines indicate ± STD. From the distribution of the residuals, it can be observed that the IMs residuals can be uniformly distributed as the epicenter distance increases, and most of them are distributed within ± STD. The best distribution is for

PGA, as it has no more discrete residual values, which can also be seen from the histogram results. The histograms of PGD, SA (1.0), and SA (3.0) show more discrete values, although their residuals are also the closest to zero. All IMs have relatively low STDs, consistent with the expected results.

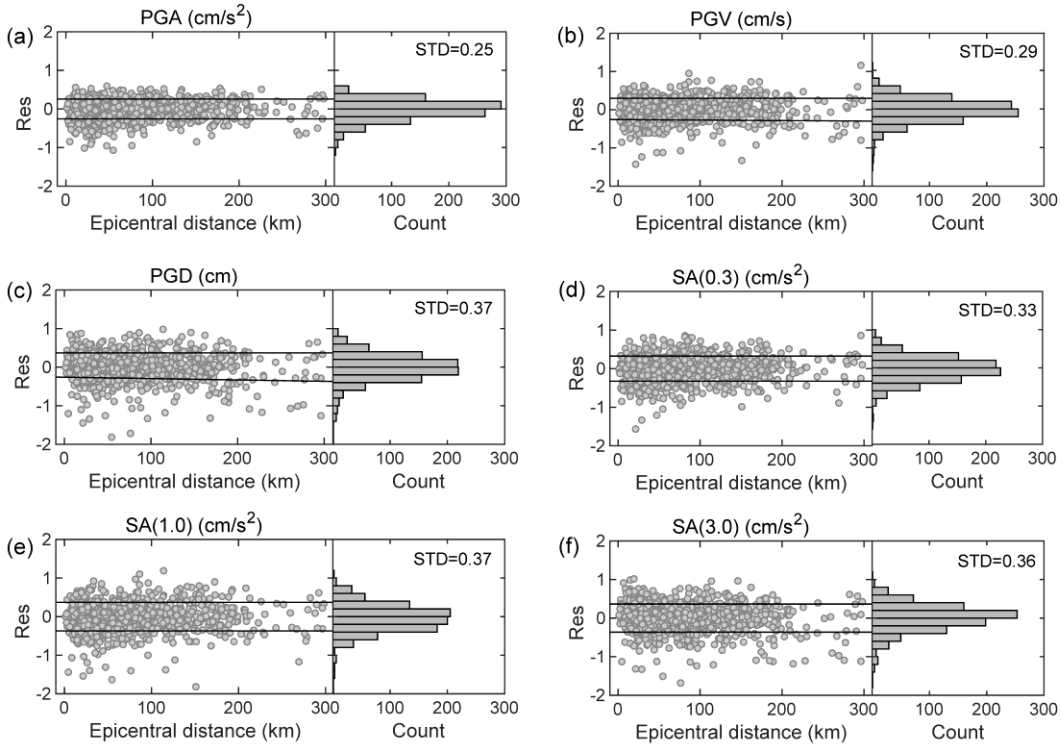

Figure 6. Predicting the distribution of IMs residuals with epicenter distance.

3.4 Predictive performance of the model at longer time windows on the test dataset

We assessed the ability of CRAQuake to predict IMs using seismic waves with longer TW (3 s to 17 s). The Res values for 5s, 10s, 15s, and 17s IMs are presented here. It is evident that they range between -1 and 1, with Res gradually decreasing as TW increases (Figure 7). Additionally, the heat maps in Figure 8 depict the results of PCCs and STD, which show an increase in PCCs (darker and darker colors) and a decrease in STD (lighter and lighter colors) as TW increases. Linear correlations between predicted and target values are also plotted (Supplementary Information, Figure S4, and S5), and as TW increases, predicted IMs are uniformly distributed on both sides of the 1:1 line. This indicates that the ability of CRAQuake to predict IMs improves with increasing TW.

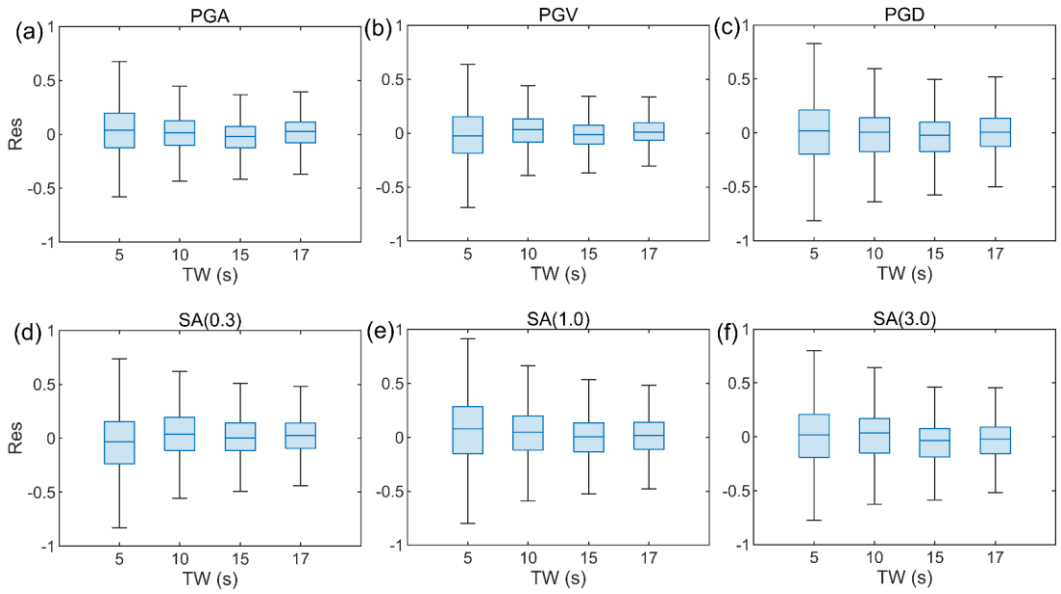

Figure 7. In the performance of CRAQuake on estimating residuals with time window growth, the box plot indicates the median, the 25th, and 75th percentiles, with the whisker extending to the minimum and maximum values that are not outliers.

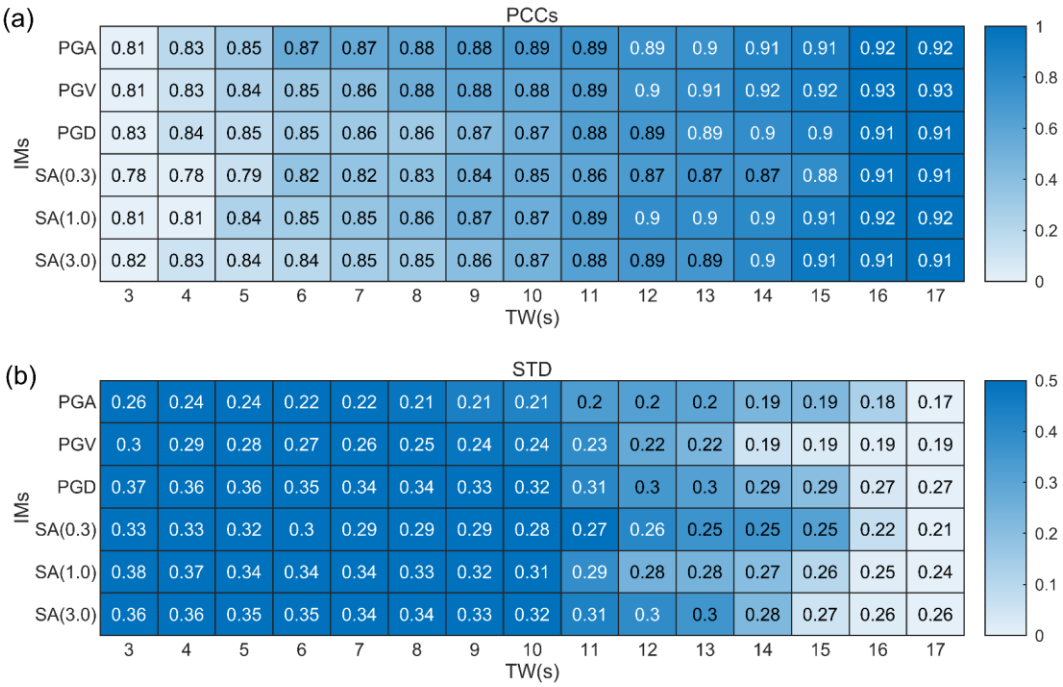

Figure 8. Results of CRAQuake in predicting PCCs and STD of IMs on the test dataset when TW is increased.

3.5 Results of CRAQuake vs. GMPE for Earthquake Events

To evaluate the effectiveness of the CRAQuake model, three earthquake events (Ms ≥ 6.5) that occurred in the North-South Seismic Belt of China were selected for testing. The predicted outcomes were compared with those of the GMPE model, and the predicted PGA and

SA results were compared with those of Zhang et al. (Zhang et al., 2022). PGA and SA GMPE models for southwest China, while the predicted PGV and PGD outcomes were compared with those of Zhang et al. (Zhang et al., 2021). PGV and PGD GMPE models for southwest China. These GMPE models were established based on seismic records in southwest China and have better accuracy and regional adaptability. Therefore, the three selected seismic events were all located in the southwest region of China (which belongs to the North-South Seismic Belt) to match the study area of Zhang et al. These three earthquakes caused significant seismic damage, including casualties, damage to houses and foundations, and secondary geologic hazards. The three earthquakes selected for the study are the 2008 Wenchuan Ms 8.0 earthquake, the 2013 Lushan Ms 7.0 earthquake, and the 2014 Ludian Ms 6.5 earthquake. The locations of the three earthquakes and the stations used are displayed in Figure 9, and additional information is available in Supplementary Information Table S5.

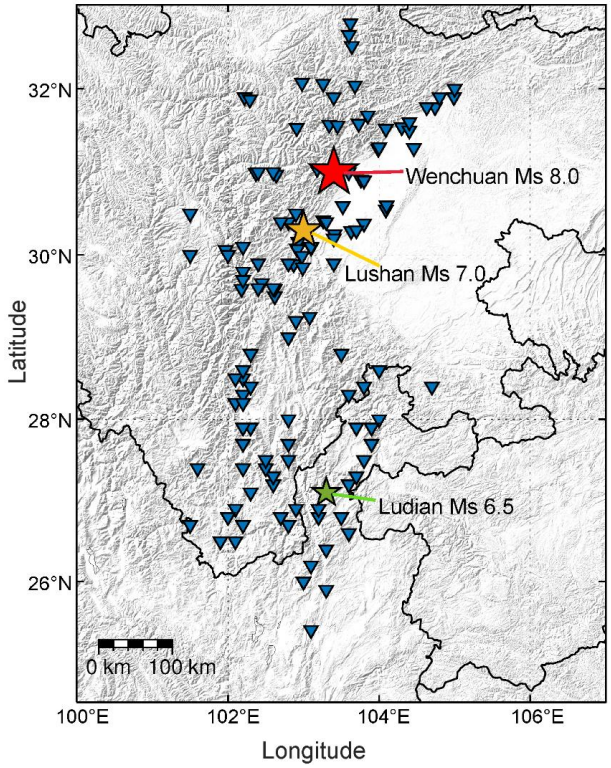

Figure 9. Distribution of epicenters and stations for typical earthquake events.

In the first testing phase, the TW it takes for a CRAQuake to reach GMPE predicted IMs STD was measured. As depicted in Figure 10, the solid black line represents the STD of the GMPE-predicted IMs, the black hollow circle represents the STD of the CRAQuake-predicted IMs, and the black pentagram indicates that the STD of the CRAQuake-predicted IMs is lower than that of the TW of the GMPE. The results show that the STD of the CRAQuake predicted IMs decreases with an increase in TW, and the STDs of the predicted IMs lower than that of GMPE are mainly concentrated within the 7s to 11s range. The shortest is 7s for PGA, the longest is 11s for SA (0.3) and SA (1.0), and the average TW is 9.5s. In the next phase, seismic waves with a TW of 10s were input into CRAQuake, and the residuals of the predicted IMs were found to be very close to those of the GMPE results and even better than those of the GMPE (Figure 11). According to the numerical results presented in Table 2, PGA, PGD, SA (0.3), and SA (3.0) are already better than GMPE. The results of PGV and SA (1.0) are also extremely

close to GMPE, which confirms the robustness of CRAQuake performance in the earthquake case test.

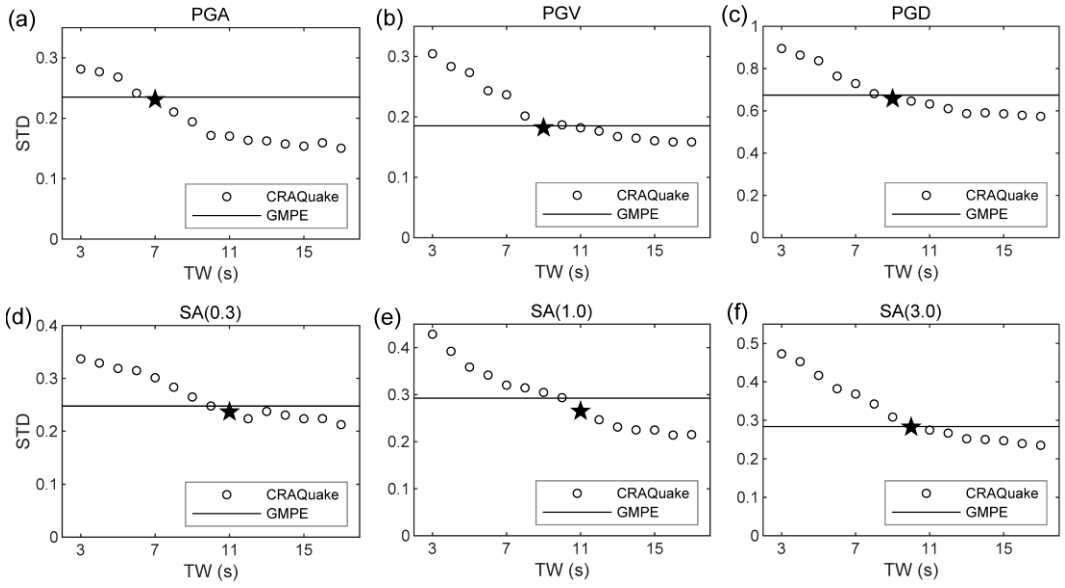

Figure 10. Evolution of STD in earthquake event testing for CRAQuake and GMPE, with the red pentagram representing the first time CRAQuake STD was lower than GMPE.

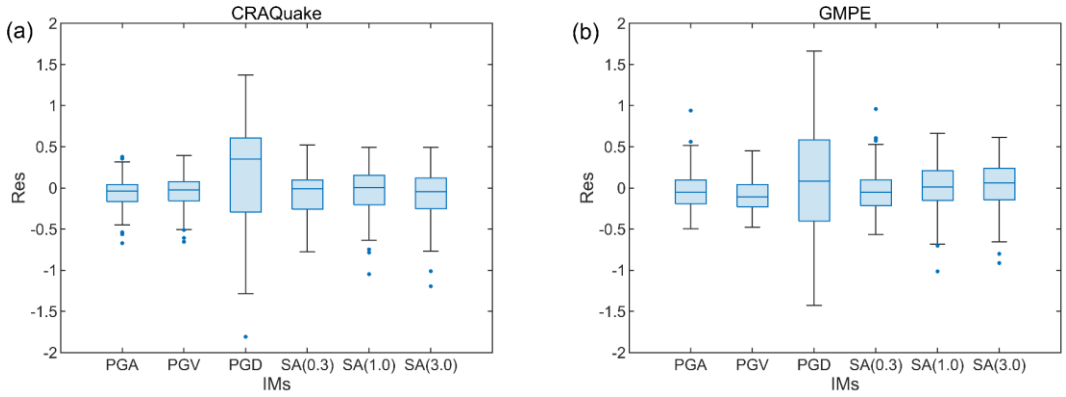

Figure 11. CRAQuake and GMPE results for predicting residuals during earthquake events; the box plot indicates the median, the 25th, and 75th percentiles with the whisker extending to the minimum and maximum values that are not outliers; dots indicate outliers.

Table 2. Comparison of CRAQuake and GMPE results for three earthquake events.

IMs	CRAQuake			GMPE		
	Median	Mean	STD	Median	Mean	STD
PGA	-0.0393	-0.0654	0.1715	-0.0507	-0.0332	0.2350
PGV	-0.0231	-0.0511	0.1868	-0.1061	-0.0894	0.1853
PGD	0.3484	0.1649	0.6462	0.0805	0.0546	0.6743
SA (0.3)	-0.0092	-0.0704	0.2477	-0.0535	-0.0511	0.2488
SA (1.0)	0.0052	-0.0360	0.2936	0.1020	-0.0022	0.2926
SA (3.0)	-0.0461	-0.0745	0.2823	0.0611	0.0371	0.2837

4 Discussion

4.1 Effect of sample size on model performance

To assess how sample size impacts CRAQuake performance. The method of Zhu et al. (Zhu et al., 2023) was referenced for this analysis. Five combinations of sample sizes were set up (Supplementary Information Table S6), and CRAQuake was trained on datasets smaller than the complete training and testing sets. Taking PGA as an example, with the model architecture and hyperparameters remaining unchanged, the standard deviation (STD) of predicted PGA gradually decreased as the number of learning samples increased (Figure 12). The supporting materials showed the same trend for other IMs, as shown in Supplementary Information Figure S6. Moreover, the downward trend of STD in Figure 12 and Figure S6 appears almost linear. This suggests that the entire training and validation datasets failed to saturate performance. Therefore, using more data would likely result in a better model. Future studies should collect more high-quality earthquake data for model training to enhance the performance of the model further.

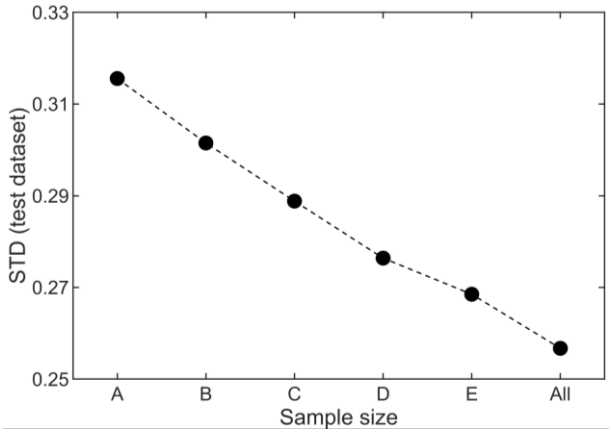

Figure 12. Impact of training and validation sample size.

4.2 Advantages over the GMPE approach and other data-driven models for prediction IMs

CRAQuake is a method that has an advantage over the GMPE approach, as it does not require complex pre-configuration of the earthquake source, path, and site terms. Instead, it only needs seismic waves recorded by a single station in the first few seconds to predict six IMs. This makes CRAQuake ideal for meeting the EEWs timeliness requirement, allowing users in the target area to respond to emergencies promptly. On the other hand, the GMPE method is highly accurate in predicting earthquakes because it uses data from multiple stations near the epicenter and considers the impact of site conditions to produce precise results. However, a challenge with this method is the unavailability of some required site parameters, which also vary across different regions and countries. For example, in Japan, the site parameter Vs30 (average shear wave velocity at 30 m depth) is more commonly used as their seismic network stations are usually drilled for wave velocity. In contrast, only a few stations in China have been surveyed for wave velocity, and the wave velocity information is only available for a depth of 20 m below the surface. As a result, CRAQuake expression without site parameters is more straightforward and can still produce reliable results similar to those of the GMPE model.

CRAQuake stands out from other IMs data-driven models(Hsu et al., 2013; Fayaz et al., 2021; Fayaz & Galasso, 2022b; Hu et al., 2022; A. Wang et al., 2023; Fayaz et al., 2023; Dai et al., 2024) in several ways. Firstly, CRAQuake does not require inputs of earthquake sources, paths, and site parameters, which allows for highly time-sensitive predictions. Secondly, its end-to-end nature eliminates the need to extract characteristic parameters from the initial arrival of the seismic wave, reducing the influence of human experience and subjectivity and resulting in more objective prediction results with less error. Additionally, the multitasking capabilities of CRAQuake enable it to predict six IMs simultaneously, making it useful for projects requiring different IMs, such as using PGA for high-speed train braking and SA for the seismic hazard analysis of building structures.

4.3 Deficiencies and Prospects

Although CRAQuake shows promising results in predicting IMs, some areas still require further investigation to enhance algorithm accuracy. For example, there is a degree of "large-value underestimation" in the PGD that CRAQuake predicts (Figure 5c). While increasing the length of the TW may improve this issue (Supplementary Information Figure S4 i - l), it may cause a delay in the warnings. To address this, subsequent research should focus on increasing the "large-value" sample size for training. Moreover, the current architecture and hyperparameters of the CRAQuake model are empirical and lack a basis in principles or rules. Therefore, further optimization of the model design is necessary to improve the prediction accuracy of the IMs. The features automatically extracted by CRAQuake from initial arrival seismic waves are unknown, and future research is needed to understand whether these features can be visualized, as in the field of image recognition (Zeiler et al., 2011), to interpret the physical meanings they represent.

5 Conclusions

In this study, we propose a multi-task integrated data-driven model called CRAQuake to improve the timeliness and accuracy of predicting IMs in the north-south seismic Belt of China. The model predicts IMs, including PGA, PGV, PGD, and SA at 0.3, 1, and 3 s periods. CRAQuake has a significant advantage in that it avoids subjectivity and bias caused by the artificial extraction of feature parameters and can fully utilize the information related to IMs in the initial arrival of seismic waves for prediction. Based on the test results, we can conclude the following:

1 CRAQuake can predict IMs rapidly and accurately without any pre-established parameters such as earthquake source, path, and site, and the effectiveness of indicating IMs improves with the increase of TW. This critical feature is indispensable for earthquake early warning and emergency response in the north-south seismic belt of China, empowering decision-makers to assess the potential impact of earthquakes and apply effective measures to minimize damage.

2 CRAQuake can predict six different IMs simultaneously, which multi-task allows the model to take full advantage of input data and improve prediction efficiency.

3 This study introduces novel approaches and concepts for predicting earthquake IMs. As data-driven methods continue to improve and advance, we anticipate that similar innovative techniques will be implemented in earthquake engineering and mitigation.

Statement

The author(s) declared no potential conflicts of interest concerning the research, authorship, or publication of this article.

Data Availability Statement

Data for this study are provided by Institute of Engineering Mechanics, China Earthquake Administration. But restrictions apply to the availability of these data, which were used under license for the current study, and so are not publicly available. Data are however available from the authors upon reasonable request and with permission of Institute of Engineering Mechanics, China Earthquake Administration. The Deep Learning Toolbox in Matlab 2023b was used to construct the CRAQuake model. Model code that can be used to reproduce the results of this paper can be found in the Zenodo repository (https://zenodo.org/records/10853378), and Matlab 2023b and the Generic Mapping Tools (GMT) were used to produce figures. Supplementary Information Tables S3 and S5 list information specific to the earthquake events used in this study. Table S2, Figure S1, and Figure S3 describe in detail the architecture of CRAQuake, the hyperparameter settings, and the training process. The GMPE model parameter settings for the comparison can be obtained from (Zhang et al., 2021) 10.6038/cjg2021O0445 and (Zhang et al., 2022) https://doi.org/10.1016/j.soildyn.2022.107297.

Acknowledgments

We want to thank the Institute of Engineering Mechanics, China Earthquake Administration. for providing data support for this study. This research was partially supported by the Key Projects of the Key Laboratory of Urban Security and Disaster Engineering of China Ministry of Education (2023), the National Key Technologies R&D Program (2023YFC3007401), and the National Natural Science Foundation of China (NSFC, Grant No. 52192675).

ORCIDIDs

Qingxu Zhao: https://orcid.org/0000-0002-8674-8057

Mianshui Rong: https://orcid.org/0000-0002-9820-0312

Bin Zhang: https://orcid.org/ 0000-0003-0466-9193

Xiaojun Li: https://orcid.org/0000-0002-7526-0558

Supplementary Information

Supplemental Information for this article is available online.

Reference

Allen, R., Gasparini, P., Kamigaichi, O., & Böse, M. (2009). The Status of Earthquake Early Warning around the World: An Introductory Overview. *Seismological Research Letters*, *80*(5), 682–693. https://doi.org/10.1785/gssrl.80.5.682

Allen, R. M., & Melgar, D. (2019). Earthquake Early Warning: Advances, Scientific Challenges, and Societal Needs. *Annual Review of Earth and Planetary Sciences*, *47*(1), 361–388. https://doi.org/10.1146/annurev-earth-053018-060457

Bazzurro, P., Cornell, C., Shome, N., & Carballo, J. (1998). Three Proposals for Characterizing MDOF Nonlinear Seismic Response. *Journal of Structural Engineering*, *124*(11). https://doi.org/10.1061/(ASCE)0733-9445(1998)124:11(1281)

Bindi, D., Pacor, F., Puglia, R., Massa, M., Ameri, G., & Paolucci, R. (2011). Ground motion prediction equations derived from the Italian strong motion database. *Bulletin of Earthquake Engineering*, *9*(6), 1899–1920. https://doi.org/10.1007/s10518-011-9313-z

Campbell, K., & Bozorgnia, Y. (2008). NGA Ground Motion Model for the Geometric Mean Horizontal Component of PGA, PGV, PGD and 5% Damped Linear Elastic Response Spectra for Periods Ranging from 0.01 to 10 s. *Earthquake Spectra*, *24*(1), 139–171. https://doi.org/10.1193/1.2857546

Campbell, K. W., & Bozorgnia, Y. (2014). NGA-West2 Ground Motion Model for the Average Horizontal Components of PGA, PGV, and 5% Damped Linear Acceleration Response Spectra. *Earthquake Spectra*, *30*(3), 1087–1115. https://doi.org/10.1193/062913EQS175M

Caruso, A., Colombelli, S., Elia, L., Picozzi, M., & Zollo, A. (2017). An on-site alert level early warning system for Italy. *Journal of Geophysical Research: Solid Earth*, *122*(3), 2106–2118. https://doi.org/10.1002/2016JB013403

China Earthquake Administration. (2020). The Chinese seismic intensity scale, GB/T 17742-2020.China Earthquake Administration, 2020. GB/T 17742-2020. The Chinese seismic

intensity scale. State Administration for Market Regulation, Standardization Administration, Beijing.

Chung, J., Gulcehre, C., Cho, K., & Bengio, Y. (2014). Empirical Evaluation of Gated Recurrent Neural Networks on Sequence Modeling. https://doi.org/110.48550/arXiv 1412.3555

Cremen, G., & Galasso, C. (2020). Earthquake early warning: Recent advances and perspectives. *Earth-Science Reviews*, *205*, 103184. https://doi.org/10.1016/j.earscirev.2020.103184

Dai, H., Zhou, Y., Liu, H., Li, S., Wei, Y., & Song, J. (2024). XGBoost-based prediction of on-site acceleration response spectra with multi-feature inputs from P-wave arrivals. *Soil Dynamics and Earthquake Engineering*, *178*, 108503. https://doi.org/10.1016/j.soildyn.2024.108503

Du, W., & Ning, C.-L. (2021). Modeling spatial cross-correlation of multiple ground motion intensity measures (SAs, PGA, PGV, Ia, CAV, and significant durations) based on principal component and geostatistical analyses. *Earthquake Spectra*, *37*(1), 486–504. https://doi.org/10.1177/8755293020952442

Fayaz, J., & Galasso, C. (2022a). A deep neural network framework for real-time on-site estimation of acceleration response spectra of seismic ground motions. *Computer-Aided Civil and Infrastructure Engineering*, mice.12830. https://doi.org/10.1111/mice.12830

Fayaz, J., & Galasso, C. (2022b). A generalized ground-motion model for consistent mainshock–aftershock intensity measures using successive recurrent neural networks. *Bulletin of Earthquake Engineering*, *20*(12), 6467–6486. https://doi.org/10.1007/s10518-022-01432-w

Fayaz, J., Xiang, Y., & Zareian, F. (2021). Generalized ground motion prediction model using hybrid recurrent neural network. *Earthquake Engineering & Structural Dynamics, 50*(6), 1539–1561. https://doi.org/10.1002/eqe.3410

Fayaz, J., Medalla, M., Torres-Rodas, P., & Galasso, C. (2023). A recurrent-neural-network-based generalized ground-motion model for the Chilean subduction seismic environment. *Structural Safety, 100*, 102282. https://doi.org/10.1016/j.strusafe.2022.102282

Festa, G., Picozzi, M., Caruso, A., Colombelli, S., Cattaneo, M., Chiaraluce, L., et al. (2017). Performance of Earthquake Early Warning Systems during the 2016–2017 Mw 5–6.5 Central Italy Sequence. *Seismological Research Letters, 89*(1). https://doi.org/10.1785/0220170150

Hajian, A., Nunnari, G., & Kimiaefar, R. (2023). Deep Learning: Applications in Seismology and Volcanology. In A. Hajian, G. Nunnari, & R. Kimiaefar (Eds.), *Intelligent Methods with Applications in Volcanology and Seismology* (pp. 103–140). Cham: Springer International Publishing. https://doi.org/10.1007/978-3-031-15432-4_5

Hochreiter, S., & Schmidhuber, J. (1997). Long Short-term Memory. *Neural Computation, 9*(8), 1735–1780. https://doi.org/10.1162/neco.1997.9.8.1735

Hsiao, N.-C., Wu, Y., Shin, T.-C., Zhao, L., & Teng, T.-L. (2009). Development of earthquake early warning system in Taiwan. *Geophysical Research Letters, 36*(2), L00B02. https://doi.org/10.1029/2008GL036596

Hsu, T.-Y., Huang, S.-K., Chang, Y.-W., Kuo, C.-H., Lin, C.-M., Chang, T.-M., et al. (2013). Rapid on-site peak ground acceleration estimation based on support vector regression and P-wave features in Taiwan. *Soil Dynamics and Earthquake Engineering, 49*, 210–217. https://doi.org/10.1016/j.soildyn.2013.03.001

Hsu, T.-Y., Lin, P.-Y., Wang, H., Chiang, H., Chang, Y., Kuo, C.-H., et al. (2018). Comparing the Performance of the NEEWS Earthquake Early Warning System Against the CWB System During the February 6 2018 Mw 6.2 Hualien Earthquake. *Geophysical Research Letters*, *45*(12), 6001–6007. https://doi.org/10.1029/2018GL078079

Hu, J., Jin, C., Zhang, H., Hu, L., & Wang, Z. (2022). Support Vector Regression for Developing Ground-Motion Models for Arias Intensity, Cumulative Absolute Velocity, and Significant Duration for the Kanto Region, Japan. *Seismological Research Letters*, *93*(3), 1619–1635. https://doi.org/10.1785/0220210259

Ji, K., Zhu, C., Yaghmaei-Sabegh, S., Lu, J., Ren, Y., & Wen, R. (2023). Site classification using deep-learning-based image recognition techniques. *Earthquake Engineering & Structural Dynamics*, *52*(8), 2323–2338. https://doi.org/10.1002/eqe.3801

Jozinović, D., Lomax, A., Štajduhar, I., & Michelini, A. (2020). Rapid prediction of earthquake ground shaking intensity using raw waveform data and a convolutional neural network. *Geophysical Journal International*, *222*(2), 1379–1389. https://doi.org/10.1093/gji/ggaa233

Kanamori, H. (2005). Real-Time Seismology and Earthquake Damage Mitigation. *Annual Review of Earth and Planetary Sciences*, *33*(1), 195–214. https://doi.org/10.1146/annurev.earth.33.092203.122626

Kingma, D. P., & Ba, J. (2017, January 29). Adam: A Method for Stochastic Optimization. arXiv. https://doi.org/10.48550/arXiv.1412.6980

Lecun, Y., Bottou, L., Bengio, Y., & Haffner, P. (1998). Gradient-Based Learning Applied to Document Recognition. *Proceedings of the IEEE*, *86*(11), 2278–2324. https://doi.org/10.1109/5.726791

512 Liu C., Li X., Jing B., Xi N., & Tian X. (2019). The distance segmentation characters of PGV-Pd
513 relationship parameters for earthquake early warning. *Chinese Journal Of Geophysics*,
514 *62*(4), 1413–1426.
515 Liu, Y., Zhao, Q., & Wang, Y. (2024). Peak ground acceleration prediction for on-site
516 earthquake early warning with deep learning. *Scientific Reports*, *14*(1).
517 https://doi.org/10.1038/s41598-024-56004-6
518 Mousavi, S. M., & Beroza, G. (2022a). Deep-learning seismology. *Science*, *377*(6607).
519 https://doi.org/10.1126/science.abm4470
520 Mousavi, S. M., & Beroza, G. (2022b). Machine Learning in Earthquake Seismology. *Annual*
521 *Review of Earth and Planetary Sciences*, *51*(1). https://doi.org/10.1146/annurev-earth-
522 071822-100323
523 Mousavi, S. M., Ellsworth, W., Weiqiang, Z., Chuang, L., & Beroza, G. (2020). Earthquake
524 transformer—an attentive deep-learning model for simultaneous earthquake detection and
525 phase picking. *Nature Communications*, *11*(3952). https://doi.org/10.1038/s41467-020-
526 17591-w
527 Münchmeyer, J., Bindi, D., Leser, U., & Tilmann, F. (2021). The transformer earthquake alerting
528 model: a new versatile approach to earthquake early warning. *Geophysical Journal*
529 *International*, *225*(1), 646–656. https://doi.org/10.1093/gji/ggaa609
530 Peng, C., Yang, J., Xue, B., Zhu, X., & Chen, Y. (2013). Exploring the feasibility of earthquake
531 early warning using records of the 2008 Wenchuan earthquake and its aftershocks. *Soil*
532 *Dynamics and Earthquake Engineering*, *57*, 86–93.
533 https://doi.org/10.1016/j.soildyn.2013.11.005

Peng, C., Yang, J., Zheng, Y., Zhu, X., Xu, Z., & Chen, Y. (2017). New τc regression relationship derived from all P-wave time windows for rapid magnitude estimation. *Geophysical Research Letters*, *44*(5). https://doi.org/10.1002/2016GL071672

Satriano, C., Elia, L., Martino, C., Lancieri, M., Zollo, A., & Iannaccone, G. (2011). PRESTo, the earthquake early warning system for Southern Italy: Concepts, capabilities and future perspectives. *Soil Dynamics and Earthquake Engineering*, *31*, 137–153. https://doi.org/10.1016/j.soildyn.2010.06.008

Vaswani, A., Shazeer, N., Parmar, N., Uszkoreit, J., Jones, L., Gomez, A. N., et al. (2017). Attention Is All You Need. arXiv. https://doi.org/10.48550/arXiv.1706.03762

Wald, D. J., Quitoriano, V., Heaton, T. H., & Kanamori, H. (1999). Relationships between Peak Ground Acceleration, Peak Ground Velocity, and Modified Mercalli Intensity in California. *Earthquake Spectra*, *15*(3), 557–564. https://doi.org/10.1193/1.1586058

Wang, A., Li, S., Jianqi, L., Zhang, H., Wang, B., & Xie, Z. (2023). Prediction of PGA in earthquake early warning using a long short-term memory neural network. *Geophysical Journal International*, *234*(1), 12–24. https://doi.org/10.1093/gji/ggad067

Wang, Y., Li, X., Li, L., Wang, Z., & Lan, J. (2021). New Magnitude Proxy for Earthquake Early Warning Based on Initial Time Series and Frequency. *Seismological Research Letters*, *93*(1), 216–225. https://doi.org/10.1785/0220210106

Wang, Y., Li, X., Wang, Z., & Liu, J. (2022). Deep learning for magnitude prediction in earthquake early warning. *Gondwana Research*, *123*, 164–173. https://doi.org/10.1016/j.gr.2022.06.009

Wang, Y., Zhao, Q., Qian, K., Wang, Z., Cao, Z., & Wang, J. (2023). Cumulative absolute velocity prediction for earthquake early warning with deep learning. *Computer-Aided Civil and Infrastructure Engineering*. https://doi.org/10.1111/mice.13065

Wu, Y., & Kanamori, H. (2005). Rapid Assessment of Damage Potential of Earthquakes in Taiwan from the Beginning of P Waves. *Bulletin of the Seismological Society of America*, *95*(3), 1181–1185. https://doi.org/10.1785/0120040193

Wu, Y., & Kanamori, H. (2008). Exploring the feasibility of on-site earthquake early warning using close-in records of the 2007 Noto Hanto earthquake. *Earth Planets and Space*, *60*, 155–160. https://doi.org/10.1186/BF03352778

Wu, Y., & Zhao, L. (2006). Magnitude estimation using the first three second P-wave amplitude in earthquake early warning. *Geophysical Research Letters*, *331*(16), L16312. https://doi.org/10.1029/2006GL026871

Wu, Y., Kanamori, H., Allen, R., & Hauksson, E. (2007). Determination of earthquake early warning parameters, τc and Pd, for southern California. *Geophysical Journal International*, *170*(2), 711–717. https://doi.org/10.1111/j.1365-246X.2007.03430.x

Zeiler, M., Taylor, G., & Fergus, R. (2011). *Adaptive Deconvolutional Networks for Mid and High Level Feature Learning*. *Proceedings of the IEEE International Conference on Computer Vision* (Vol. 2011, p. 2025). https://doi.org/10.1109/ICCV.2011.6126474

Zhang, B., Yu, Y., Li, X., Wang, Y., & Rong, M. (2021). Ground motion attenuation relationship of horizontal component of PGV and PGD in southwest China. *Chinese Journal Of Geophysics*, *64*(8), 2733–2748.

Zhang, B., Yu, Y., Li, X., & Wang, Y. (2022). Ground motion prediction equation for the average horizontal component of PGA, PGV, and 5% damped acceleration response

spectra at periods ranging from 0.033 to 8.0s in southwest China. *Soil Dynamics and Earthquake Engineering*, *159*, 107297. https://doi.org/10.1016/j.soildyn.2022.107297

Zhu, C., Cotton, F., Kawase, H., & Bradley, B. (2023). Separating broad-band site response from single-station seismograms. *Geophysical Journal International*, *234*(3), 2053–2065. https://doi.org/10.1093/gji/ggad187

Zollo, A., Iannaccone, G., Lancieri, M., Cantore, L., Convertito, V., Emolo, A., et al. (2009). Earthquake early warning system in southern Italy: Methodologies and performance evaluation. *Geophysical Research Letters*, *36*(4), L00B07. https://doi.org/10.1029/2008GL036689

Zollo, A., Amoroso, O., Lancieri, M., Wu, Y., & Kanamori, H. (2010). A Threshold-based Earthquake Early Warning using dense accelerometer networks. *Geophysical Journal International*, *183*(2), 963–974. https://doi.org/10.1111/j.1365-246X.2010.04765.x

Zollo, A., Colombelli, S., Caruso, A., & Elia, L. (2023). An Evolutionary Shaking-Forecast-Based Earthquake Early Warning Method. *Earth and Space Science*, *10*(4), e2022EA002657. https://doi.org/10.1029/2022EA002657

Figure 1.

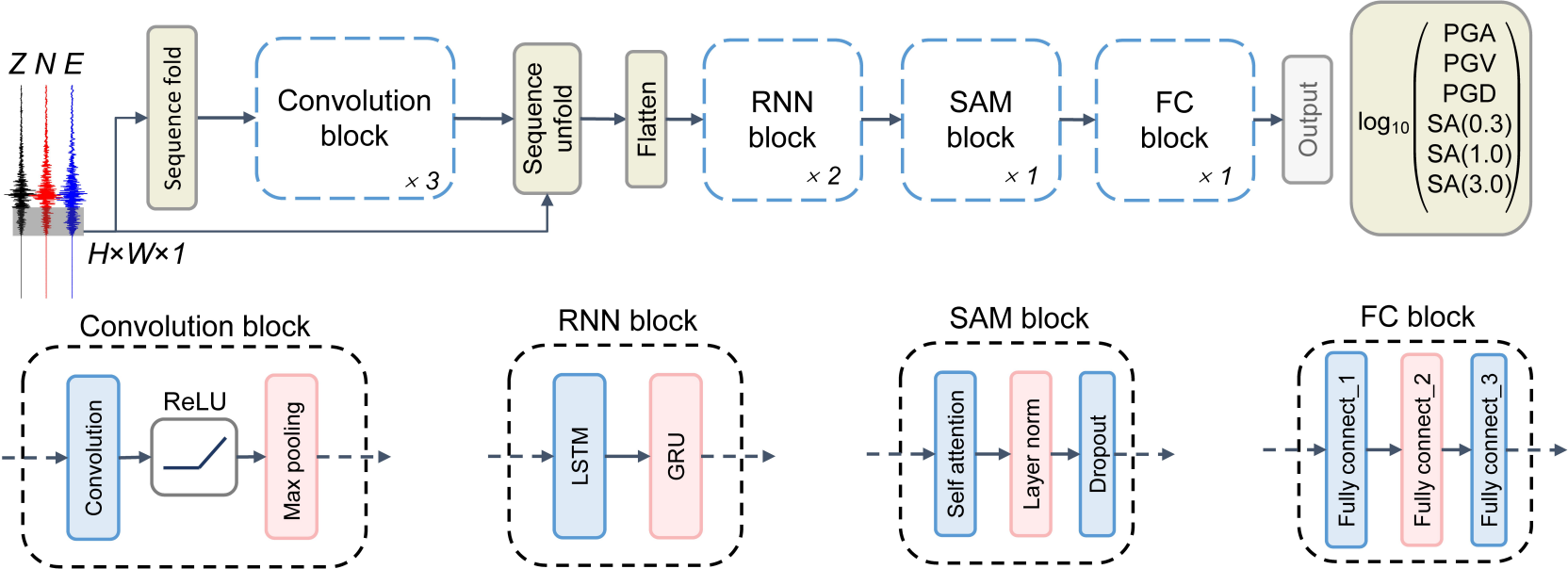
Z N E
H×W×1
Sequence fold
Convolution block
× 3
Sequence unfold
Flatten
RNN block
× 2
SAM block
× 1
FC block
× 1
Output
log10
PGA
PGV
PGD
SA(0.3)
SA(1.0)
SA(3.0)
Convolution block
Convolution
ReLU
Max pooling
RNN block
LSTM
GRU
SAM block
Self attention
Layer norm
Dropout
FC block
Fully connect_1
Fully connect_2
Fully connect_3

Figure 2.

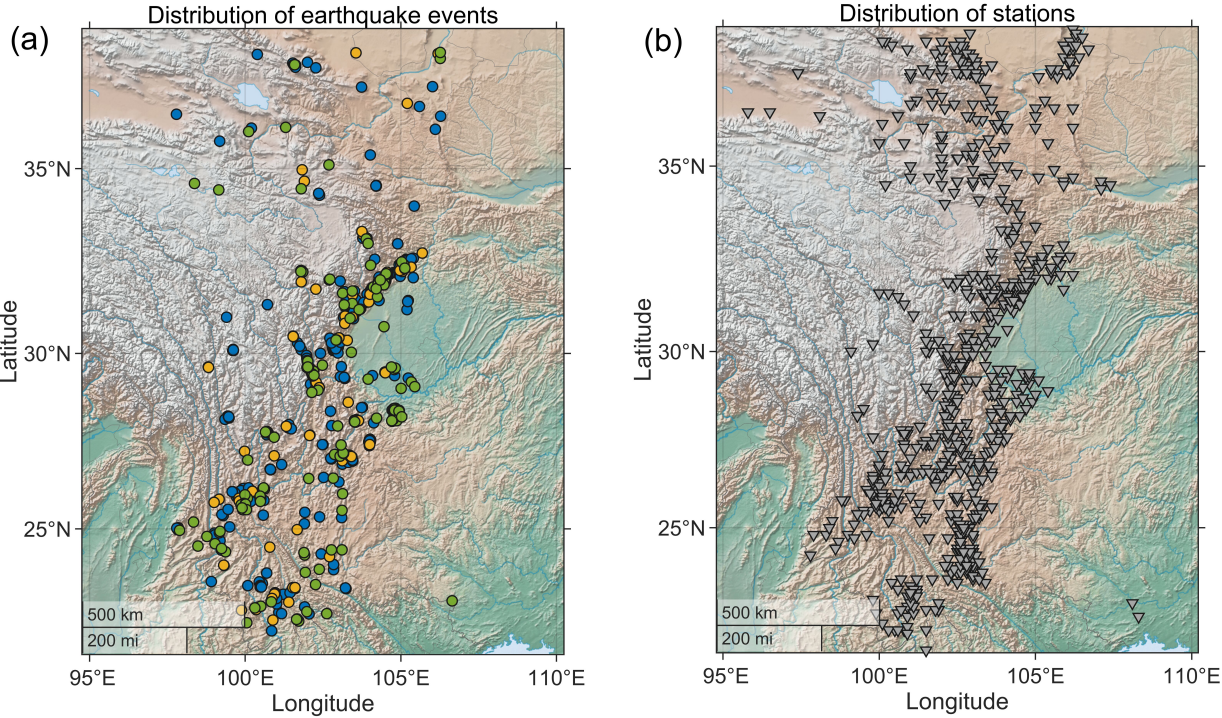
(a)
Distribution of earthquake events
35°N
30°N
25°N
Latitude
500 km
200 mi
95°E
100°E
105°E
110°E
Longitude
(b)
Distribution of stations
35°N
30°N
25°N
Latitude
500 km
200 mi
95°E
100°E
105°E
110°E
Longitude
Train
Validate
Test
Station

Figure 3.

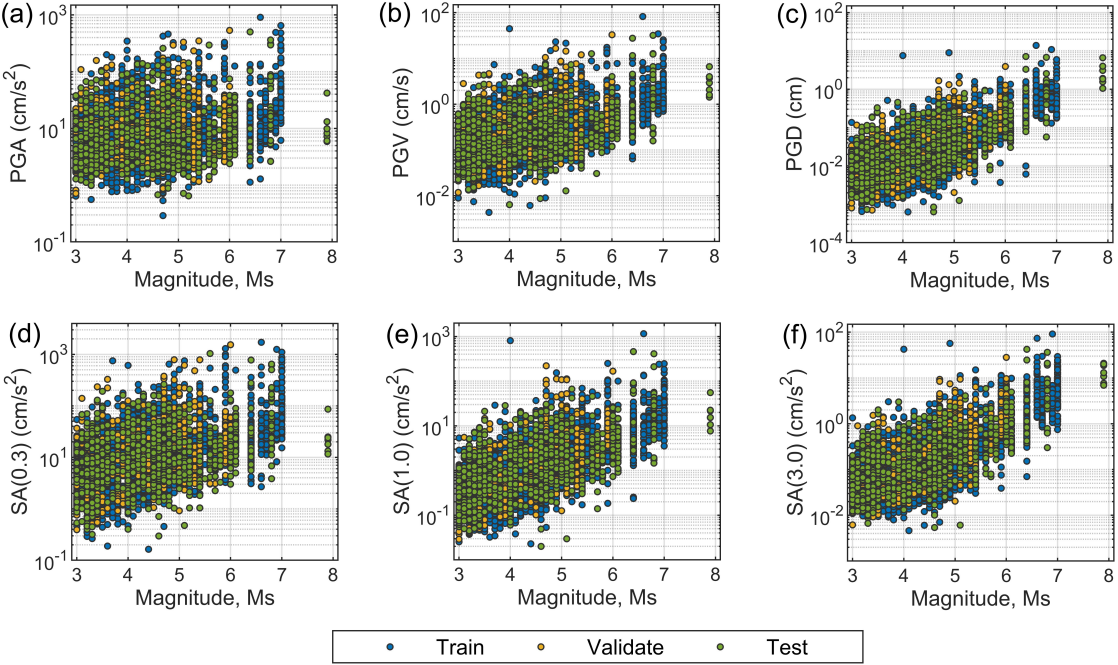
(a)
PGA (cm/s^2)
Magnitude, Ms
(b)
PGV (cm/s)
Magnitude, Ms
(c)
PGD (cm)
Magnitude, Ms
(d)
SA(0.3) (cm/s^2)
Magnitude, Ms
(e)
SA(1.0) (cm/s^2)
Magnitude, Ms
(f)
SA(3.0) (cm/s^2)
Magnitude, Ms
Train
Validate
Test

Figure 4.

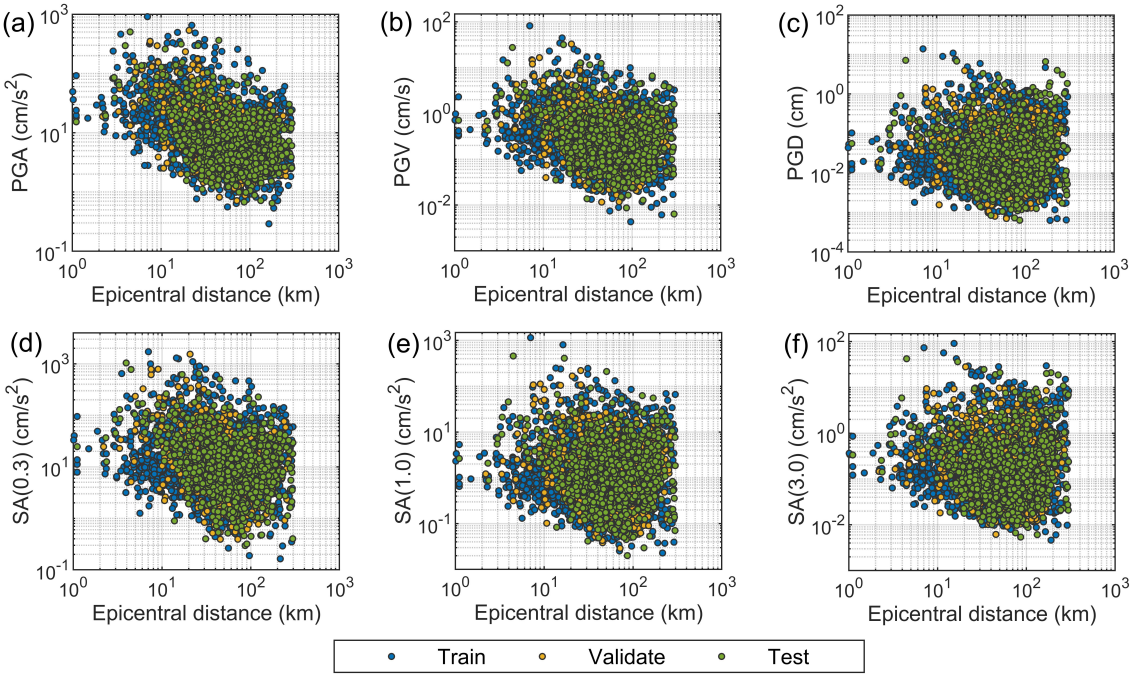
(a)
PGA (cm/s^2)
Epicentral distance (km)
(b)
PGV (cm/s)
Epicentral distance (km)
(c)
PGD (cm)
Epicentral distance (km)
(d)
SA(0.3) (cm/s^2)
Epicentral distance (km)
(e)
SA(1.0) (cm/s^2)
Epicentral distance (km)
(f)
SA(3.0) (cm/s^2)
Epicentral distance (km)
Train
Validate
Test

Figure 5.

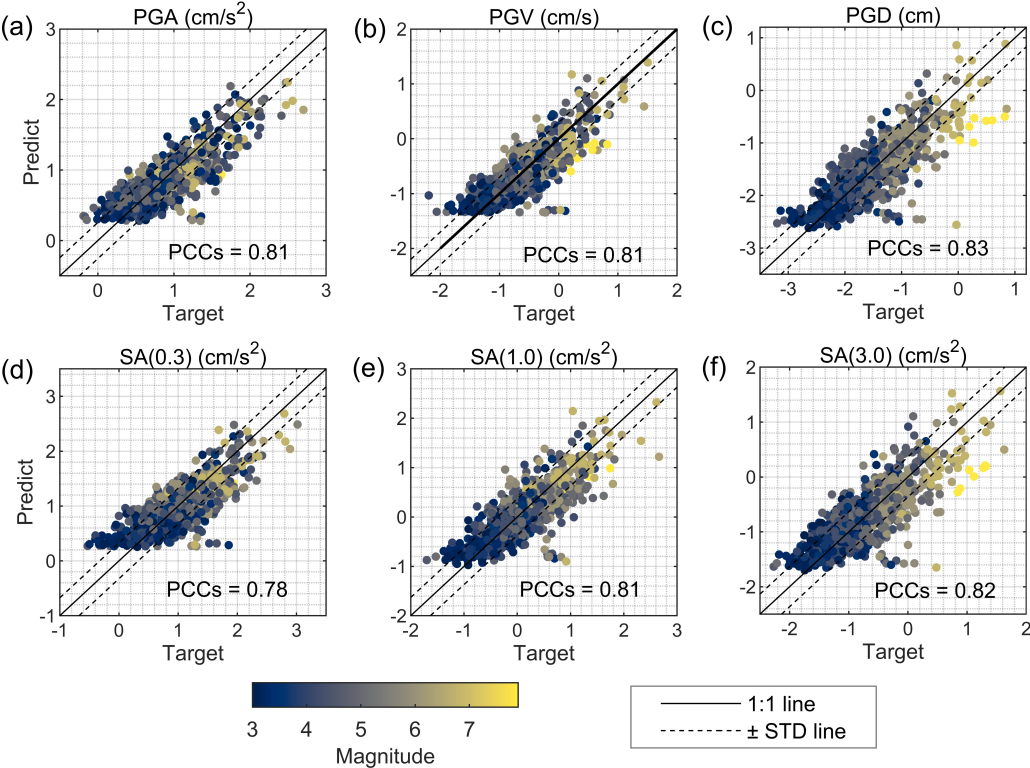
(a)
PGA (cm/s^2)
Predict
Target
PCCs = 0.81
(b)
PGV (cm/s)
Target
PCCs = 0.81
(c)
PGD (cm)
Target
PCCs = 0.83
(d)
SA(0.3) (cm/s^2)
Predict
Target
PCCs = 0.78
(e)
SA(1.0) (cm/s^2)
Target
PCCs = 0.81
(f)
SA(3.0) (cm/s^2)
Target
PCCs = 0.82
3 4 5 6 7
Magnitude
1:1 line
± STD line

Figure 6.

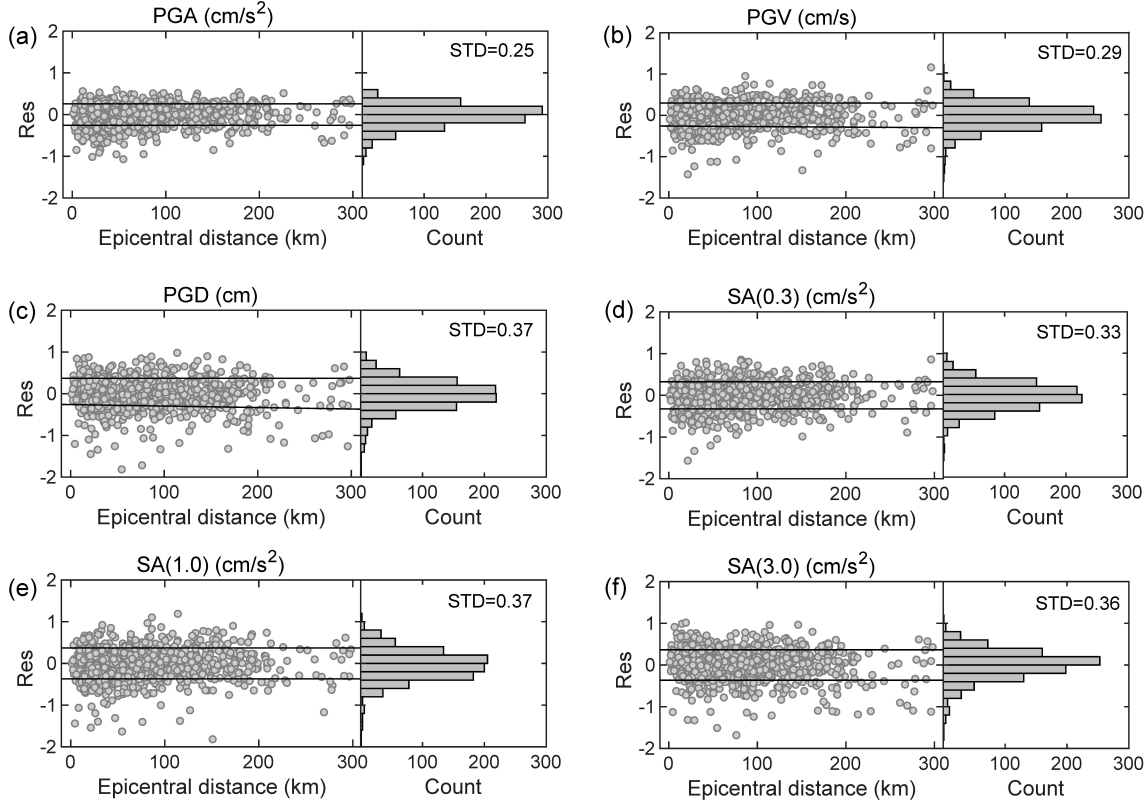
(a)
PGA (cm/s^2)
STD=0.25
(b)
PGV (cm/s)
STD=0.29
(c)
PGD (cm)
STD=0.37
(d)
SA(0.3) (cm/s^2)
STD=0.33
(e)
SA(1.0) (cm/s^2)
STD=0.37
(f)
SA(3.0) (cm/s^2)
STD=0.36
Res
Epicentral distance (km)
Count

Figure 7.

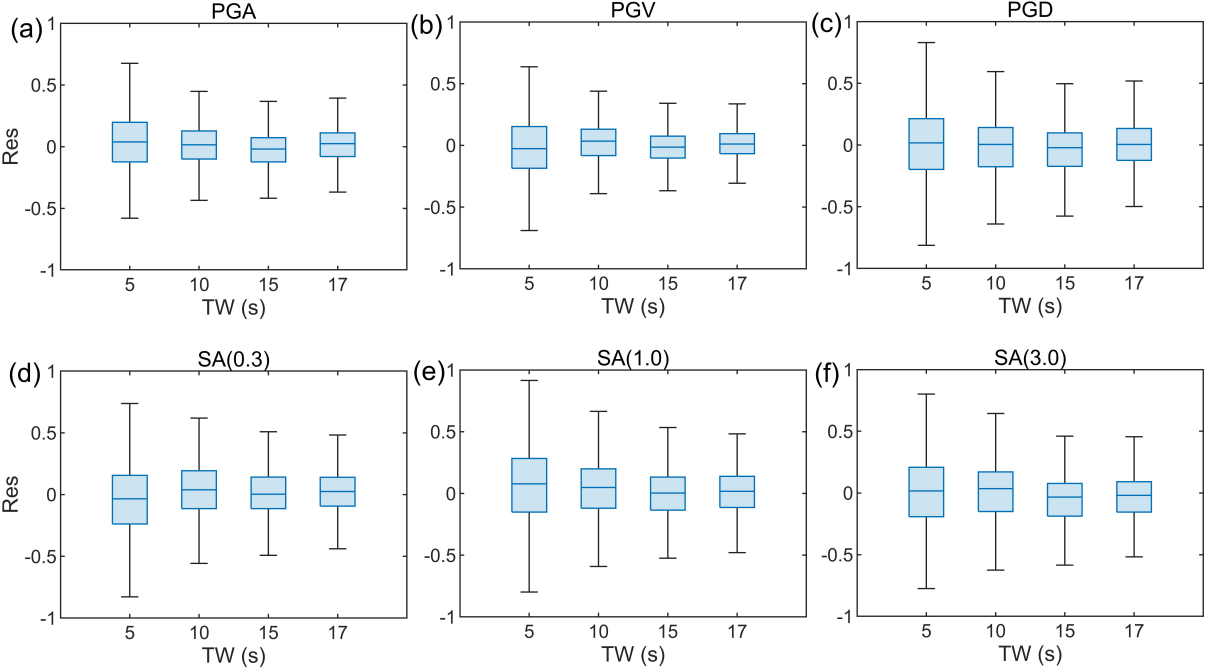
(a)
PGA
(b)
PGV
(c)
PGD
(d)
SA(0.3)
(e)
SA(1.0)
(f)
SA(3.0)
Res
TW (s)
1
0.5
0
-0.5
-1
5
10
15
17

Figure 8.

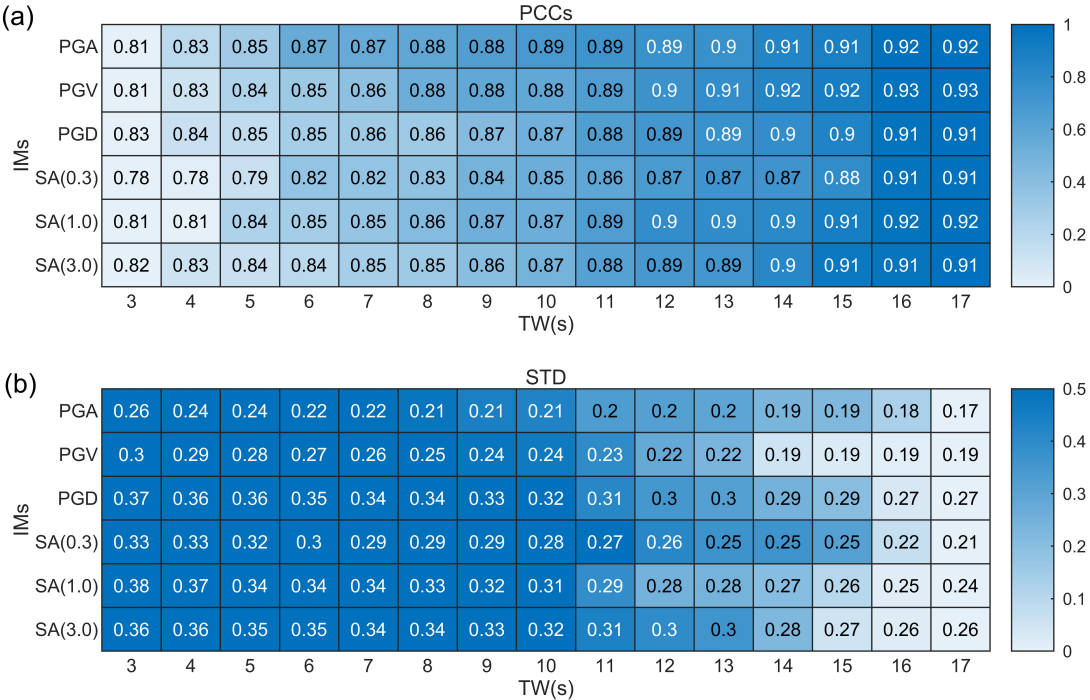
(a)
PCCs
IMs
PGA 0.81 0.83 0.85 0.87 0.87 0.88 0.88 0.89 0.89 0.89 0.9 0.91 0.91 0.92 0.92
PGV 0.81 0.83 0.84 0.85 0.86 0.88 0.88 0.88 0.89 0.9 0.91 0.92 0.92 0.93 0.93
PGD 0.83 0.84 0.85 0.85 0.86 0.86 0.87 0.87 0.88 0.89 0.89 0.9 0.9 0.91 0.91
SA(0.3) 0.78 0.78 0.79 0.82 0.82 0.83 0.84 0.85 0.86 0.87 0.87 0.87 0.88 0.91 0.91
SA(1.0) 0.81 0.81 0.84 0.85 0.85 0.86 0.87 0.87 0.89 0.9 0.9 0.9 0.91 0.92 0.92
SA(3.0) 0.82 0.83 0.84 0.84 0.85 0.85 0.86 0.87 0.88 0.89 0.89 0.9 0.91 0.91 0.91
3 4 5 6 7 8 9 10 11 12 13 14 15 16 17
TW(s)
1 0.8 0.6 0.4 0.2 0
(b)
STD
IMs
PGA 0.26 0.24 0.24 0.22 0.22 0.21 0.21 0.21 0.2 0.2 0.2 0.19 0.19 0.18 0.17
PGV 0.3 0.29 0.28 0.27 0.26 0.25 0.24 0.24 0.23 0.22 0.22 0.19 0.19 0.19 0.19
PGD 0.37 0.36 0.36 0.35 0.34 0.34 0.33 0.32 0.31 0.3 0.3 0.29 0.29 0.27 0.27
SA(0.3) 0.33 0.33 0.32 0.3 0.29 0.29 0.29 0.28 0.27 0.26 0.25 0.25 0.25 0.22 0.21
SA(1.0) 0.38 0.37 0.34 0.34 0.34 0.33 0.32 0.31 0.29 0.28 0.28 0.27 0.26 0.25 0.24
SA(3.0) 0.36 0.36 0.35 0.35 0.34 0.34 0.33 0.32 0.31 0.3 0.3 0.28 0.27 0.26 0.26
3 4 5 6 7 8 9 10 11 12 13 14 15 16 17
TW(s)
0.5 0.4 0.3 0.2 0.1 0

Figure 9.

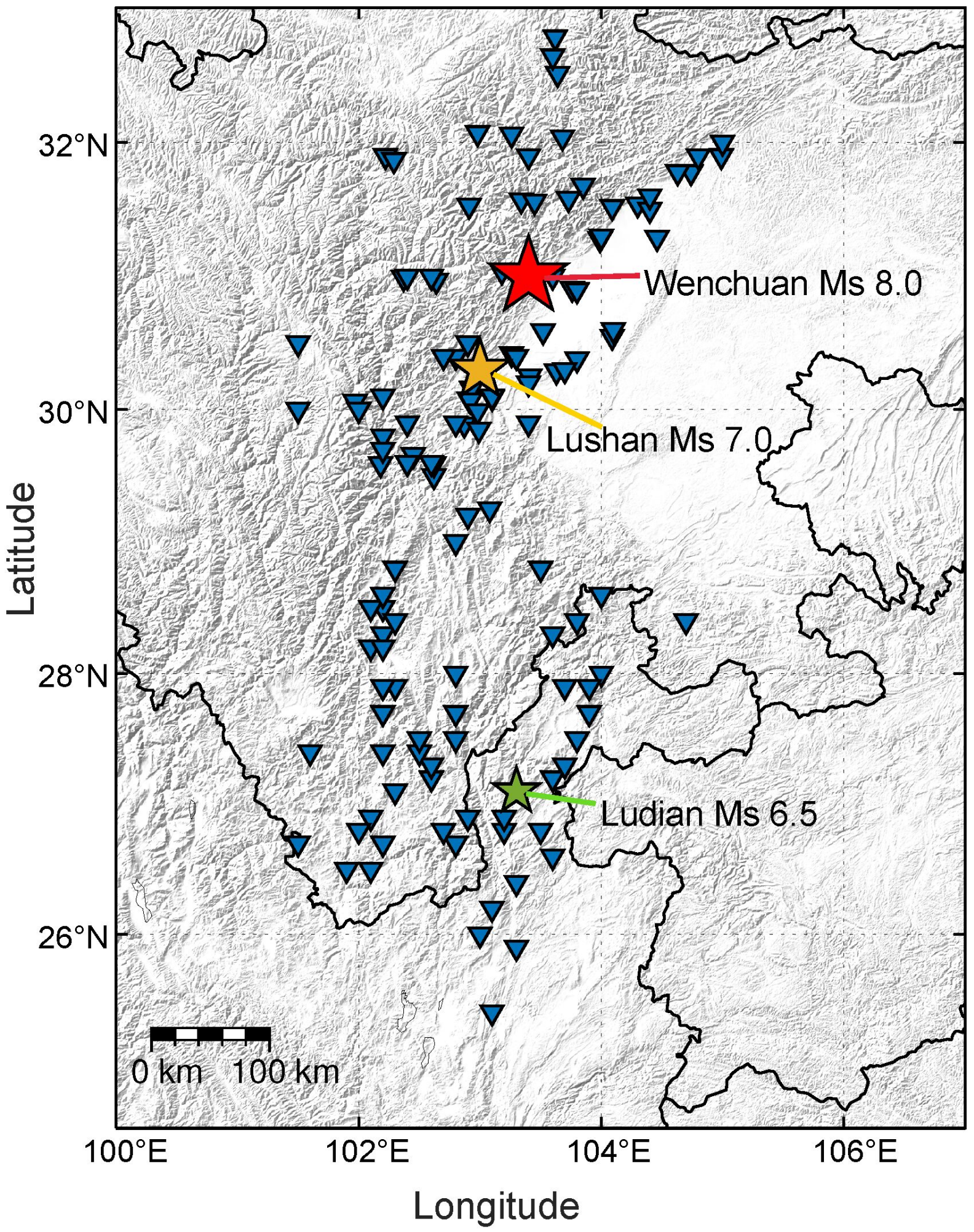
Wenchuan Ms 8.0
Lushan Ms 7.0
Ludian Ms 6.5
32°N
30°N
28°N
26°N
100°E
102°E
104°E
106°E
Latitude
Longitude
0 km
100 km

Figure 10.

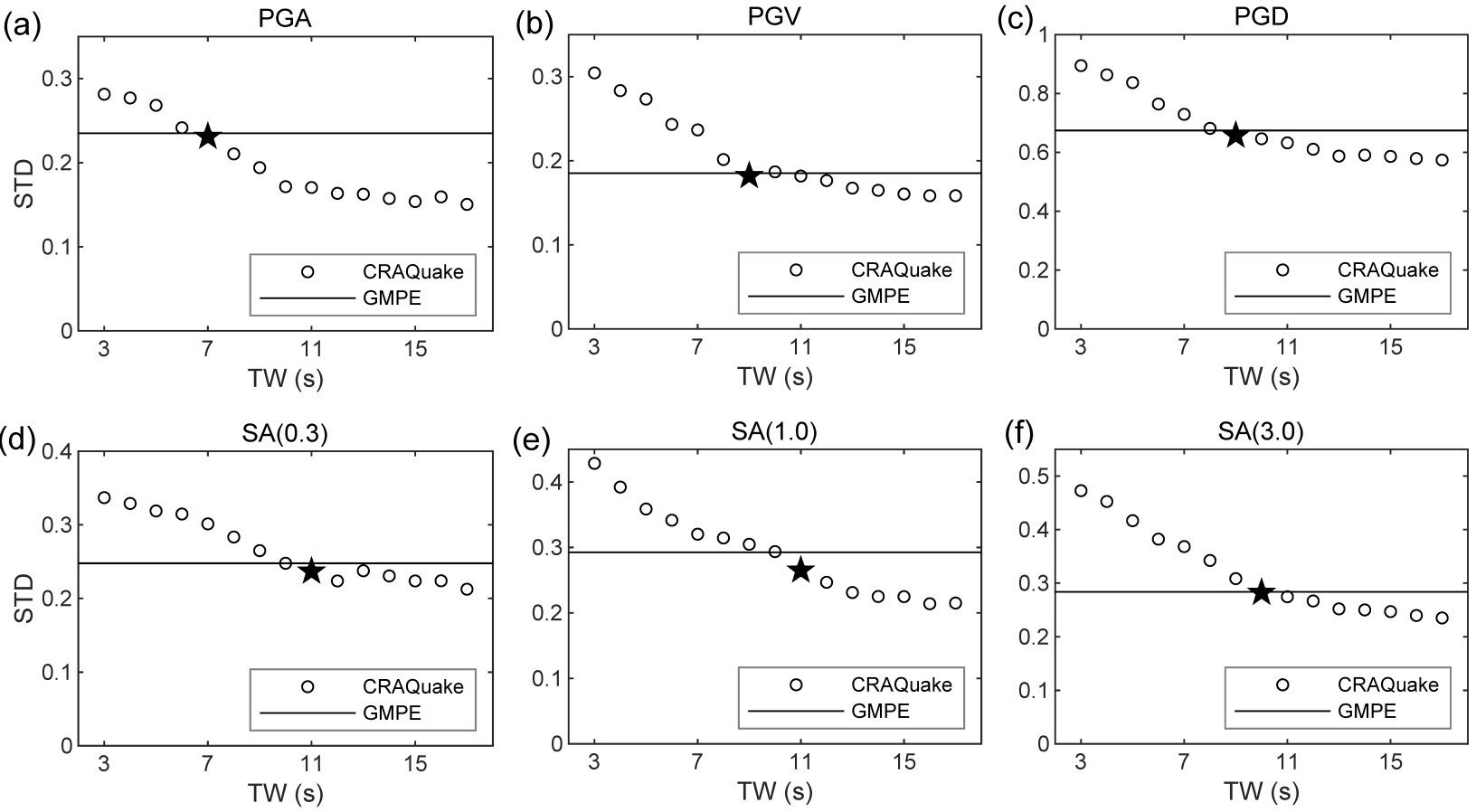
(a)
PGA
(b)
PGV
(c)
PGD
(d)
SA(0.3)
(e)
SA(1.0)
(f)
SA(3.0)
STD
TW (s)
CRAQuake
GMPE

Figure 11.

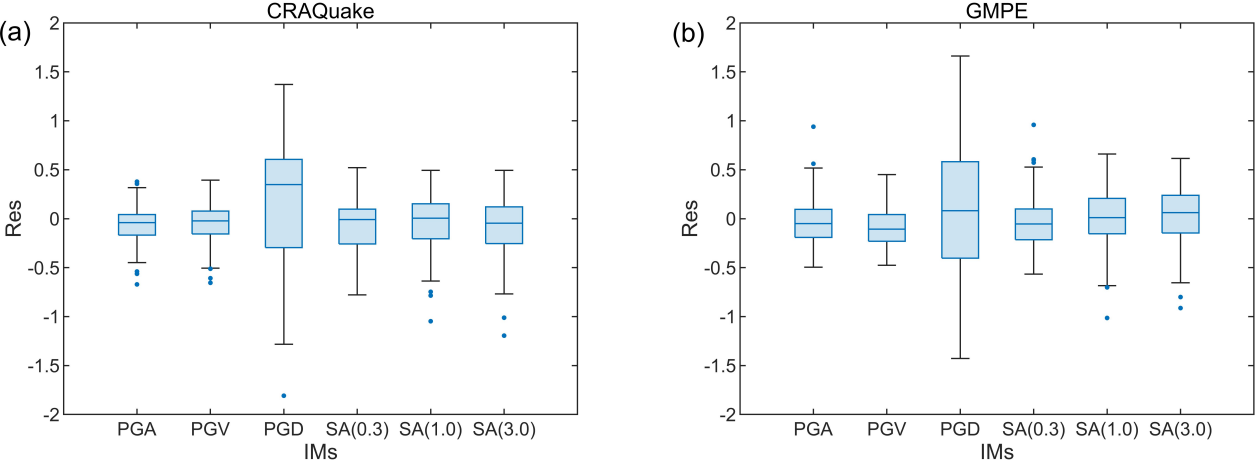
(a)
CRAQuake
Res
IMs
PGA
PGV
PGD
SA(0.3)
SA(1.0)
SA(3.0)
(b)
GMPE
Res
IMs
PGA
PGV
PGD
SA(0.3)
SA(1.0)
SA(3.0)

Figure 12.

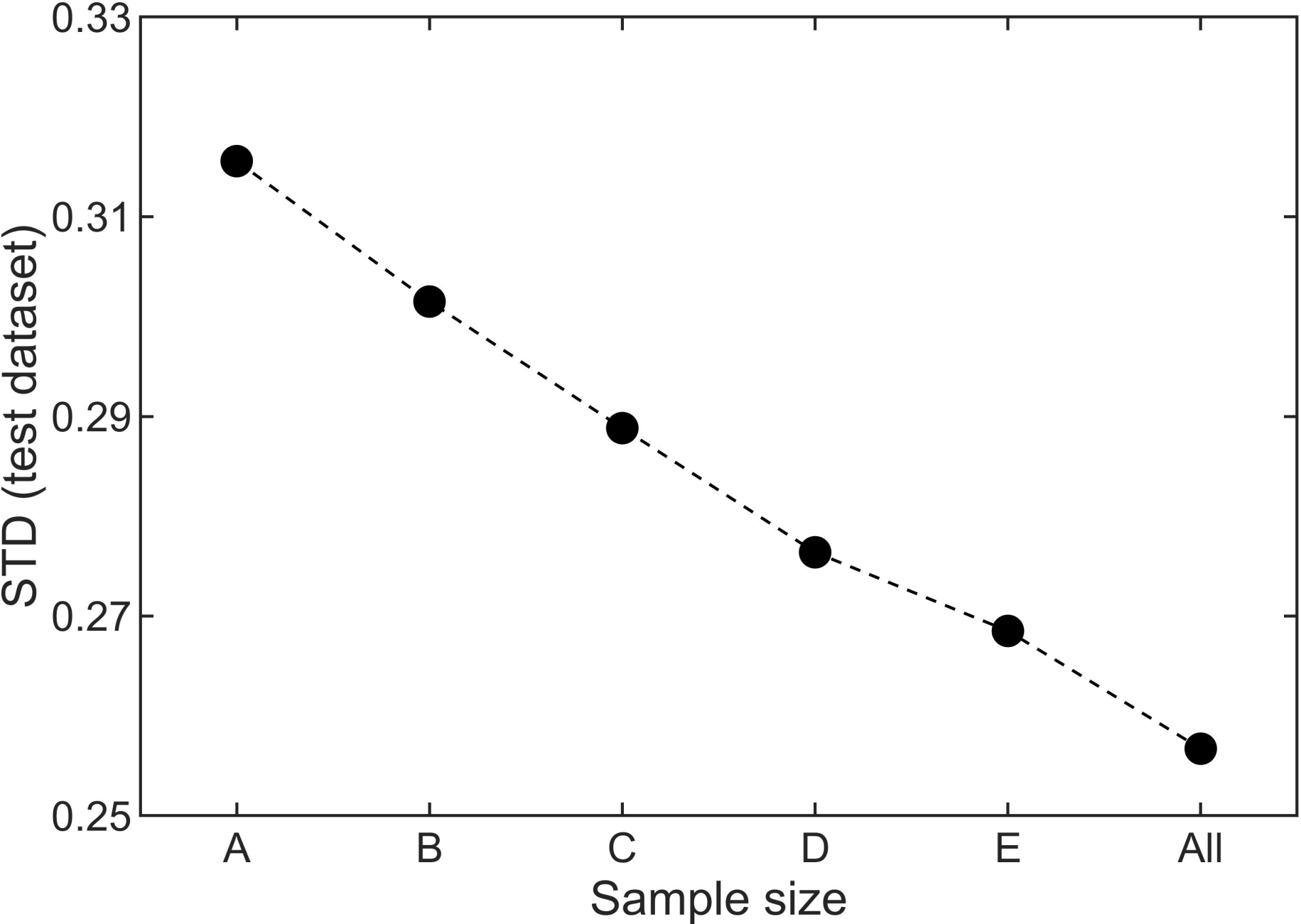
0.33
0.31
0.29
0.27
0.25
STD (test dataset)
A
B
C
D
E
All
Sample size